AFRL-AFOSR-VA-TR-2022-0332

A 4D Nanoprinter for Making and Manipulating Macroscopic Materials

Mirkin, Chad
NORTHWESTERN UNIVERSITY
633 CLARK
EVANSTON, IL, 60208
USA

06/30/2022
Final Technical Report

Air Force Research Laboratory
Air Force Office of Scientific Research
Arlington, Virginia 22203
Air Force Materiel Command

REPORT DOCUMENTATION PAGE

PLEASE DO NOT RETURN YOUR FORM TO THE ABOVE ORGANIZATION.

1. REPORT DATE	2. REPORT TYPE	3. DATES COVERED	
		START DATE	END DATE
20220630	Final	20151215	20211214

4. TITLE AND SUBTITLE
A 4D Nanoprinter for Making and Manipulating Macroscopic Materials

5a. CONTRACT NUMBER	5b. GRANT NUMBER	5c. PROGRAM ELEMENT NUMBER
	FA9550-16-1-0150	61102F
5d. PROJECT NUMBER	**5e. TASK NUMBER**	**5f. WORK UNIT NUMBER**

6. AUTHOR(S)
Chad Mirkin

7. PERFORMING ORGANIZATION NAME(S) AND ADDRESS(ES)
NORTHWESTERN UNIVERSITY
633 CLARK
EVANSTON, IL 60208
USA

8. PERFORMING ORGANIZATION REPORT NUMBER

9. SPONSORING/MONITORING AGENCY NAME(S) AND ADDRESS(ES)
Air Force Office of Scientific Research
875 N. Randolph St. Room 3112
Arlington, VA 22203

10. SPONSOR/MONITOR'S ACRONYM(S)
AFRL/AFOSR RTB2

11. SPONSOR/MONITOR'S REPORT NUMBER(S)
AFRL-AFOSR-VA-TR-2022-0332

12. DISTRIBUTION/AVAILABILITY STATEMENT
A Distribution Unlimited: PB Public Release

13. SUPPLEMENTARY NOTES

14. ABSTRACT
Multi-functional 3D nanostructures have attracted significant attention in recent years due to their potential impact on fields ranging from artificial tissues, and biosensors, to metamaterials. However, to realize their full potential, new chemistries and tools for fabricating both hard and soft functional materials with nanoscale resolution are required. While current printing tools are well established for fabricating 2D hard materials, they are often materials limited, have poor resolution, or are low in throughput. We hypothesize that cantilever-free scanning probe lithography (CF-SPL), specifically polymer pen lithography (PPL) and beam pen lithography (BPL), are uniquely positioned to address these challenges and will enable the printing of functional 3D (or 4D) structures. PPL and BPL both use an array of millions pyramidal pens to deliver inks or perform localized reactions resulting in the patterning of nanostructures across cmscale areas. Using the PPL and BPL platforms, we proposed to develop innovative ink chemistries and printing methods towards the goal of building a 4D nanoprinter, which has enabled the creation of functional 3D architectures that can be applied in electronics, adaptive optical materials, and biological studies.

15. SUBJECT TERMS

16. SECURITY CLASSIFICATION OF:			17. LIMITATION OF ABSTRACT	18. NUMBER OF PAGES
a. REPORT	b. ABSTRACT	c. THIS PAGE		
U	U	U	UU	47

19a. NAME OF RESPONSIBLE PERSON	19b. PHONE NUMBER *(Include area code)*
BENNETT IBEY	000-0000

Cover Page
To: technicalreports@afsor.af.mil
Subject: Final Report
Contract/Grant Title: A 4D Nanoprinter for Making and Manipulating Macroscopic Materials
Contract / Grant #: FA9550-16-1-0150
Reporting Period: 12/15/2015 – 12/14/2021

Contents

REPORT ABSTRACT

Multi-functional 3D nanostructures have attracted significant attention in recent years due to their potential impact on fields ranging from artificial tissues, and biosensors, to metamaterials. However, to realize their full potential, new chemistries and tools for fabricating both hard and soft functional materials with nanoscale resolution are required. While current printing tools are well established for fabricating 2D hard materials, they are often materials limited, have poor resolution, or are low in throughput. We hypothesize that cantilever-free scanning probe lithography (CF-SPL), specifically polymer pen lithography (PPL) and beam pen lithography (BPL), are uniquely positioned to address these challenges and will enable the printing of functional 3D (or 4D) structures. PPL and BPL both use an array of millions pyramidal pens to deliver inks or perform localized reactions resulting in the patterning of nanostructures across cm-scale areas. Using the PPL and BPL platforms, we proposed to develop innovative ink chemistries and printing methods towards the goal of building a 4D nanoprinter, which has enabled the creation of functional 3D architectures that can be applied in electronics, adaptive optical materials, and biological studies.

ACCOMPLISHMENTS

Research Objectives:

TA1: Synergistic Efforts for Architecture

- Yr1-3: Mirkin and Braunschweig to design and fabricate a beam pen lithography system with a million actuated pens and sub-diffraction limited resolution.
- Yr1-3: Mirkin, Wang, and Brown to fabricate photoactuatable pen arrays (pPPL) that have one million individually addressable pens that can pattern nanoscale amounts of hard and soft materials over macro scale ranges.
- Yr1-3: Mirkin and Braunschweig to integrate individual tip actuation with a microfluidic cell to print hard and soft materials in a single macro scale array with nanoscale resolution.
- Yr3-5: Collaboration between all group for the integration of pen architectures with orthogonal photo-active ink libraries (TA2) to produce multifunctional materials with sub-diffraction limit resolution in both 2D and 3D.
- Yr3-5: Brown to develop cantilever-free scanning probe microscopy for massively parallel surface imaging.
- Yr3-5: Mirkin to investigate bulk additive manufacturing towards the invention of new technology for high-area rapid 3D printing.

TA2: Synergistic Efforts for Ink Chemistry

- Yr1-3: Design orthogonal libraries of inks with functional properties including conducting (Wang), biological (Mrksich), responsive (Gianneschi), and structural (Braunschweig) that are tailored for beam pen lithography (Mirkin).
- Yr2: Collaborate with Griep (ARL) to accelerate sensing initiatives pursued by the DoD.
- Yr2-5: Braunschweig and Mrksich to create carbohydrate arrays for exploring fundamental questions in glycobiology.
- Yr3-5: Mirkin and Gianneschi to characterize and develop a range of patternable inks using Liquid Cell TEM (LCTEM)
- Yr3-5: Braunschweig and Wang will create templated hierarchical arrays of aligned nanotubes.

- Yr3-5: Wang and Gianneschi will explore the incorporation of photolabile groups to control nanoscale surface chemistry to explore nanostructures as photosensitizers to drive chemical reactions on surfaces.
- Yr3-5: Collaboration with Mirkin, Braunschweig, Gianneschi, Mrksich, and Wang for the integration of pen architectures with orthogonal photo-active ink libraries to produce multifunctional materials with sub-diffraction limit resolution in both 2D and 3D.

Details of accomplishments:

2016:

With recent breakthroughs in cantilever-free lithography, it is now possible to cheaply and efficiently pattern nanostructures over square centimeter areas by the direct deposition of materials with polymer pen lithography (PPL) and via the delivery of energy to a substrate with beam pen lithography (BPL). These methods allow for controlled deposition of sub-100 nm features in a two-dimensional plane. Here, we have sought to build upon these platforms to increase not only their addressable area and resolution, but also print multifunctional materials in a three-dimensional arrangement. We have employed a synergistic approach that combines the expertise in nanoscale lithography (**Mirkin**) and surface-based chemistry (**Braunschweig**) with solution-based chemistry of multi-stimuli responsive (**Gianneschi**), electrical (**Wang**), and biological (**Mrksich**) materials. Utilizing this expertise, we have prototyped designs of a new inverted cantilever-free system for continuous printing and a fluid cell that can be integrated to our scanning probe instruments for precise volume control and multiplex ink delivery. Our efforts have also focused on designing novel inks that have orthogonal chemistries, including synthesizing protein building blocks to assemble biocompatible megamolecules, introducing fluorescent quantum defects in carbon nanotubes for electronic applications, and synthesizing highly controlled polymer inks using ROMP and RAFT polymerization reactions. Through the synthesis and characterization of these novel inks in our new 4D nanoprinter, nanomaterial fabrication can be tuned for desired material properties.

2017:

In 2017, the **Mirkin** group utilized an inverted, beam-pen lithography (BPL) interface to fabricate macroscale 3D prints from a variety of polymer resins. The **Braunschweig** group developed a viable solution to the tip based lithography (TBL) multiplexing challenge. By combining microfluidics, BPL, and surface organic chemistry, they showed that each tip can print patterns composed of multiple different inks with features as small as 2 μm. The **Gianneschi** group developed methods to print 20 nm gold features onto silicon nitride membranes for imaging DNA-directed self-assembly in collaboration with the **Mirkin** lab. The **Brown** group joined the MURI this year and invented a new pen array architecture that allows the user to determine when each pen is in contact with the surface which is critical to improve registration accuracy. Additionally, significant work was carried out on photo-actuated polymer pen lithography (pPPL) through direct and indirect methods. The **Mirkin** group used light as a switch to activate an actuation mechanism that results in heating and thus expansion of the polymer array. The **Wang** and **Brown** groups uncovered the mechanism behind a CNT-PDMS based composite pen array that is capable of photo-actuated printing and showed that local illumination is capable of moving these pens by as much as 3 μm. The **Mrksich** group created new bioactive ink molecules, based on megamolecule protein technology, that are monodisperse, large (10-100 nm), non-linear, programmable in their

connectivity, and functionalized with fluorescent proteins that can pattern proteins with submicron resolution. The **Gianneschi** group designed UV-responsive cyclic pro-gelator peptides as smart inks for beam pen-guided self-assembly of peptide hydrogels. Additionally, they began building an opto-fluidic device to investigate the effects of non-equilibrium driving forces on the final state of macro-molecular aggregation. The **Wang** group developed a light-driven chemistry for creation of quantum emitting sites on a carbon semiconductor substrate.

2018:

In 2018, the **Brown**, **Wang**, and **Mirkin** groups made breakthroughs in array architecture and composition towards the goal of achieving the actuation of individual pens to write patterns of arbitrary complexity. In addition, the **Mirkin** group made significant advances in the creation of a CF-SPL electrochemical 3D printer using a hydrogel PPL architecture. A multiplexed flow-through printer for creating polymer brush patterns with control over height and composition in the *x*, *y*, and *z* dimensions was developed by the **Braunschweig** group and integrated with the existing BPL platform. The **Brown** group invented an approach for determining tip-sample contact using thin film interference, which could enable CF-SPL to also become an imaging tool. The **Mrksich** group developed methods for patterning multiple functional protein inks in three-dimensional space with nanoscale resolution. By modulating the arrangement of extracellular matrix proteins, they worked with the **Mirkin** group to study cell differentiation. The pursuit of nanoscale 3D printing inspired the **Mirkin** group to develop a new high-area rapid printing (HARP) 3D printer. This year, fluid flow technology was integrated into the HARP 3D printer improving heat management and enabling record high volumetric throughput, 3.75 ft^3/h.

Substantial progress was made in the synthesis and understanding of inks for nanostructure fabrication along with their integration into both 2D and 3D printers. The **Braunschweig** group utilized a multiplexed printer to study polymer brush formation through surface-initiated atom-transfer radical polymerization. Then, the **Gianneschi** group utilized matrix-assisted laser desorption/ionization imaging mass spectrometry (MALDI-IMS) to study these polymer brushes. The **Braunschweig** group also investigated the viability of synthesizing glycan arrays that will be used to answer fundamental questions in glycobiology. The **Wang** group developed a light-driven chemistry for covalently attaching functional molecular groups on carbon substrates. The **Mrksich** group synthesized a series of large (10-100 nm) protein megamolecule inks with programmable connectivity towards the goal of patterning single molecules using BPL. The **Mirkin** group combined patterning with a bioinspired, tunable scaffold to develop a platform to grow and modulate cells. The **Gianneschi** group showed the soft-matter processes can be monitored *in situ* using liquid cell transmission electron microscopy and in collaboration with the **Mirkin** group, they are using this platform to investigate the nucleation and assembly of another ink, the programmable atom equivalent.

2019:

In 2019, the **Wang** and **Brown** groups have made strides towards achieving photo-actuated PPL at the individual pen level through a combination of theoretical and experimental studies. This work guided modifications to the 4D printer design resulting in the actuation of a 3 × 3 array of pens. Additionally, they have realized structurally isolated pen arrays which greatly reduced the crosstalk between pens. They have also taken advantage of the high thermal expansion of air to create a novel elastomer backing layer system with air-filled cavities capable of high actuation efficiencies. In other architectural advancements, the **Mirkin** group created a trapped-fluid array

holder which enabled the incorporation of a reference electrode into the electrochemical PPL, this will allow us to precisely monitor current flow and study ion transfer, features necessary for the printing of 3D metallic structures. In addition, during the development of the high area rapid printer, the **Mirkin** group studied the fluid flow across the interface and investigated the structural and mechanical fidelity of the printed parts. Importantly, these studies resulted in the launch of Azul3D, a startup based on technology developed in this MURI. The **Braunschweig** and **Gianneschi** groups created a platform for patterning light-responsive brush polymers in an O_2-free chamber, and discovered that feature height can be precisely controlled through light intensity. Lastly, an innovative imaging technique has emerged from the **Brown** group in collaboration with **TERA-Print** to use the massively parallel PPL architecture as an imaging platform with sub-10 nm resolution.

Substantial progress was made towards the synthesis of novel inks as well as their integration into the 4D printer. The **Mirkin** group worked in collaboration with the **Gianneschi** group to study photopolymeric materials such as hydrogels and peptide-polymers. These hydrogels were used to study cellular migration by controlling local mechanical properties to recapitulate the natural extracellular matrix. The **Wang** group found that light can be used to locally activate and functionalize a diazoether isomer onto carbon nanotube substrates using a Raman laser. The **Mrksich** group developed a new solid-phase synthesis for building hierarchical bioinks with precisely-defined nanoscale architectures using fusion proteins and linkers with the goal of patterning single molecules on substrates with the **Mirkin** group. The **Braunschweig** and **Giannechi** groups collaborated to pattern and characterize actuatable thermoresponsive inks such as dimethylacrylamide and N,N-isopropylylacrylamide.

2020:

On the architectural side, the **Wang** and **Brown** groups, in collaboration with the **Mirkin** group, designed a novel pen array architecture for the independent actuation of PPL pens that uses a thermally insulating backing layer and a novel light absorbing layer, and this design resulted in a doubling of the actuation efficiency and a simultaneously suppression in the thermal crosstalk. Additionally, the **Brown** and **Wang** groups invented a novel imaging tool, cantilever-free atomic force microscopy (CF-AFM). For the first time, they achieved topographical imaging in a massively parallel (cm-scale) format with sub-10 nm resolution. Towards the printing of high-resolution multi-functional 3D polymeric structures, the **Braunschweig** group, together with the **Gianneschi** group and **TERA-print**, successfully integrated a BPL pen array with advanced optics and microfluidics into the printer and used it to study controlled-surface polymerization. In addition, the **Mirkin** group developed a new technique, termed electrochemical polymer pen lithography, where hydrogel PPL arrays were used to perform localized electrodeposition of 2D/3D metallic structures. Lastly, the **Mirkin** and **Mrksich** groups developed methods for patterning functional protein inks and found that cytoskeletal tension imposed by PPL patterned ligand arrangements can actively regulate cellular uptake.

Significant progress was also made towards the synthesis of new ink chemistries. Towards functional optoelectronic patterning, the **Wang**, **Mirkin**, and **Brown** groups developed a light-driven ink chemistry that allows for BPL patterning of covalently attached small organic molecules as fluorescent color centers on carbon nanotube substrates. The **Braunschweig** group studied the kinetics of N,N-dimethylacrylamide and N-isopropylacrylamide polymerizations in collaboration with the **Gianneschi** group to pattern thermoresponsive materials that were used to generate multi-layer encrypted messages. Furthermore, the **Mirkin** and **Gianneschi** groups collaborated to

synthesize and pattern photo-responsive hydrogels and peptide-based polymers. These soft materials served as scaffolds to study cellular migration where local mechanical properties were tuned via BPL. Finally, the **Mrksich** group developed a megamolecule strategy to tune protein scaffolds that resulted in enhanced enzymatic conversion efficiency and molecular recognition.

2021:

In the no cost extension (NCE) period, the **Brown** group explored iteratively writing and characterizing patterned polymers, photocuring them, and then characterize their mechanical properties, and therefore performing materials synthesis and characterization using the same system in a closed-loop fashion. Using methods developed in the previous year, the **Mirkin** and **Mrksich** groups further explored the application of functional protein inks to study cytoskeletal tension imposed on cells by PPL patterned substrates. In the efforts for ink chemistry development, the **Braunschwig** group utilized novel printing tools and polymer chemistries to further explore stimuli responsive hypersurfaces and glycan microarrays. Additionally, the **Gianneschi, Mirkin,** and **Braunschweig** groups explored light-triggered polymerization as a method of 3D surface patterning. Finally, the Mrksich group elaborated on previous work with developed a new bioink chemistry based on the covalent linkage of Cellular Retinoic Acid Binding Protein 2 (CRABP2), characterizing its kinetics, structure, and applications.

Dissemination of results:

The results of these efforts have been disseminated through various forms. Nearly 100 peer-reviewed papers have been published that acknowledge this award, and more are expected in the coming months. Additionally, several patents, many of them licensed, were filed, and 14 inventions were disclosed. Finally, the PIs and the trainees involved in this work have presented these findings at conferences to national and international audiences.

IMPACTS

Development of discipline(s) of the project and other disciplines:

With the development and breakthroughs achieved in cantilever-free lithography, it is now possible to pattern nanostructures cheaply and efficiently over square centimeter areas by the direct deposition of materials with polymer pen lithography (PPL), and via the delivery of energy to a substrate with beam pen lithography (BPL). These methods allow for controlled deposition of sub-100 nm features in a two-dimensional plane. We also demonstrated macroscale fabrication through development of a high-area rapid 3D printing (HARP) method.

Describe the impact on the development of human resources:

As a direct result of this funding, numerous students and young investigators have received advanced training in interdisciplinary research, including postdocs, graduate students, and staff scientists. Since the beginning of the grant, numerous graduate students have successfully defended their PhD and gone on to industrial or academic positions. Thus, this effort is making a substantial impact on increasing participation in the sciences and maintaining US competitiveness in STEM.

Describe the impact on teaching and educational experiences:

This award has had a substantial impact on teaching and educational experiences at the participating institutions. This project brings together several of the top research institutions and experts in chemistry and materials science, enhancing the experience, educational opportunities, and diverse backgrounds and perspectives. In addition, the interdisciplinary nature of the research enhances educational opportunities for researchers at the university and industrial level. This project brings together researchers with backgrounds in chemistry, engineering, and materials science. To achieve the project outcomes, they must all learn about each other's work and fields.

Describe the impact on infrastructure:

Nothing to report.

Impact on society beyond science and technology:

By expanding the capabilities of cantilever-free scanning probe lithographies, namely high-resolution printing, the advances in from this research and technological advancements will gain significant interest and adoption from researchers in new industries, such as synthetic biology, tissue engineering, biotech and pharma, agriculture, electronics, and adaptive optical materials.

CHANGES

Changes in approach:

Nothing to report

Problems or delays

Nothing to report

Expenditure impacts

Nothing to report

Significant changes in the use or care of human subjects, vertebrate animals and/or biohazards

Nothing to report

Changes to the primary place of performance from that originally proposed

Nothing to report

TECHNICAL SUMMARY AND UPDATES

PART I: Summary of Accomplishments Over the Lifetime of the Grant (2015-2020)

TA1: Architecture and Process

Fabricating Beam Arrays of Millions of Pyramids with Uniform Apertures

PI: Mirkin

Polymer pen lithography (PPL) and beam pen lithography (BPL) provide a universal platform that enables nanoscale patterning of a diverse library of materials and structures. The pyramidal shape and structure of the pens provide the optimal architecture that enables cantilever-free lithographic technologies, such as PPL and BPL, to pattern nanoscale features with precise control over registration and resolution.[1, 2] Over the lifetime of this grant we have made substantial progress developing beam pen lithography (BPL) into a nanoscale patterning technique with exquisite control over material composition and size. The key discovery that now makes BPL readily usable is the reliable, high-yielding fabrication of apertures at the tips of pyramidal pens (**Figure 1A**). In this strategy, fluorinated oils are coated on top of the pen array, and the high viscosity creates a meniscus at each pen tip. Since meniscus interactions occur only at the tip, this coating eliminates any effects due to errors in pen height, resulting in highly selective etching to give a 266 nm aperture size with variance of only 3-9% across millions of pens. Furthermore, the oil coating acts as a protective layer to make an anti-fouling interface during patterning, which prevents adhesion between pens and polymer ink and enables the patterning of larger

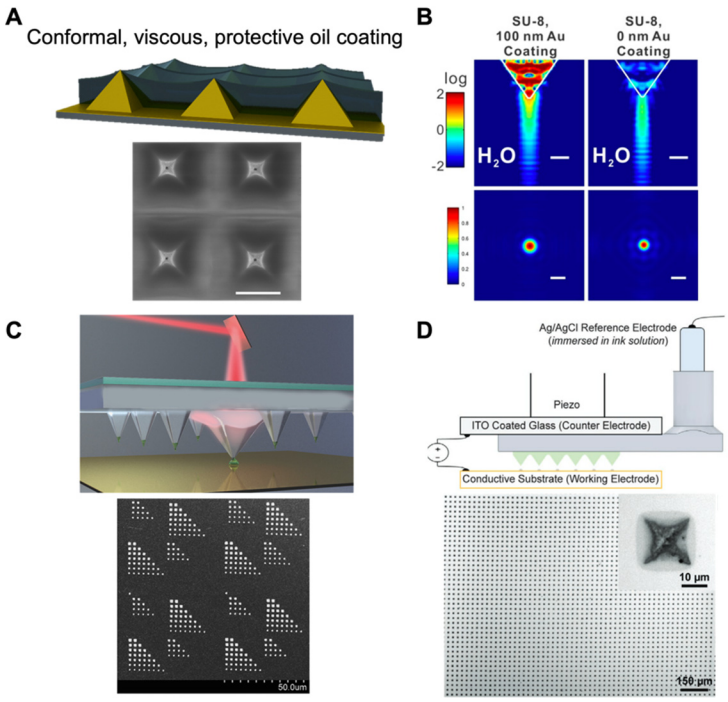

Figure 1. (**A**) Viscous oil coatings on top of pyramidal gold pens create a conformal layer to expose only the pen tips for etching and precise aperture formation while also acting as a protective anti-fouling layer. (**B**) Finite-difference time-domain (FDTD) simulations for light propagation (λ = 400 nm) in an aqueous environment (n = 1.34) through SU-8 polymer tips (n = 1.65) with 100 nm Au coating (left) and without metal coating (right), respectively. The intensity scales are normalized to the intensity at the 500 nm propagation length in each figure so that intensity profiles below the tips are obvious. The top view images of light spots are obtained at the 500 nm propagation length. Scale bars: 500 nm. (**C**) Site specific light irradiation on the back of a polymer pen array can induce strain changed causing physical extension of the specific pens for patterning on the surface. The photoactuation magnitude can be controlled to give patterns with different feature sizes. (**D**) Schematic showing the ePPL configuration with hydrogel pens containing metal precursors. Optical micrograph of a large-area pattern of >10 µm Ni-Co electrodeposited features. The large feature size enables accurate elemental characterization. Inset shows a single feature.

nanoscale features. This work was also an inspiration for the development of high-area rapid 3D printing (*i.e.,* HARP, described in a later section) that makes use of viscous oils also pursued in this grant.[3] This aperture fabrication technique was further improved using poly(methyl methacrylate) (PMMA) films to achieve uniform aperture formation down to 111 nm.

With the ability to fabricate arrays containing millions of uniform pens and apertures, we incorporated a digital micromirror device (DMD) in the light path before the pen array to control illumination at individual pen tips. This approach allows patterning of arbitrary features with independent control of chemical composition, size, and height at each pixel of the centimeter-scale substrate. Combining this precise control over patterning with microfluidic reagent delivery enables nanoscale multiplexed printing in a technique we term *The Nanosizer*, which is a breakthrough in achieving 4-dimensional printing at the nanoscale.

Rather than fabricating pen arrays that require selective tip etching for aperture formation, we have developed new pen array materials that allow BPL without the need for apertures.[4] This relies on the use of pyramidal pens made from high refractive index polymers coated with or without metal (**Figure 1B**). Total internal reflection causes focusing of light towards the pen tip, even in the absence of a metal coating, eliminating the need for a physical aperture and thus simplifying fabrication. Furthermore, removing the metal coating drastically increases the light intensity used to pattern at the tips, increasing the speed at which features are created.

Electrochemical Polymer Pen Lithography

PI: Mirkin

Despite advances in using soft organic molecules as inks or ink precursors, patterning hard materials or using metallic inks represents a new challenge when patterning at the nanoscale. To accomplish this, we developed an electrochemical polymer pen lithography (ePPL) technique that delivers metal ions to the substrate and uses an applied voltage to reduce these ion precursors into metallic patterns (**Figure 1D, Figure 2**).[5] Pens made of a soft material, such as a hydrogel, are used as microfluidic delivery systems to continuously deliver metal ion-containing inks to the pen tips. First, a hydrogel pen array is swelled with this ink and connected to an electrode. A conductive substrate is used as the working electrode. Then, when the pen tips are touched to the surface, an electrochemical cell is created. An applied potential leads to electrochemical reduction of cations in the hydrogel pen tips onto the working electrode substrate. We have demonstrated ePPL for the patterning of Ni, Pt, and Ag metals as well as NiCo alloys with control over the position, width, and height of the metal features. More than 10,000 pens were used simultaneously to electrodeposit metals ranging from 10-210 μm diameters and up to 900 nm in height.

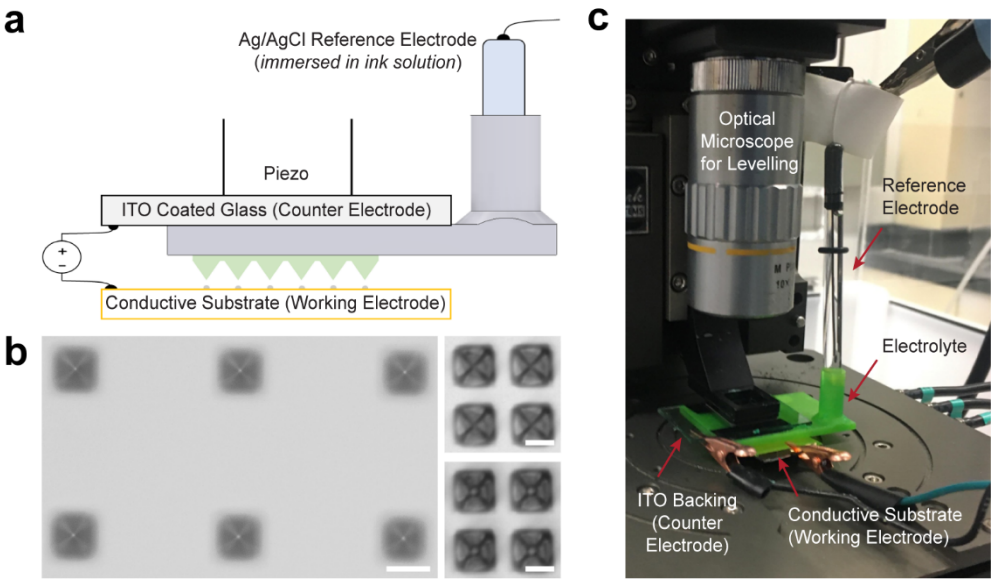

Figure 2. Experimental setup of ePPL. (a) Schematic of a three-electrode cell designed to hold the hydrogel array, electrolyte, and reference and counter electrodes in place during patterning. (b) Optical image of fabricated polyacrylamide hydrogel pen arrays, which were prepared by curing the hydrogel within a silicon master (scale bar = 30 μm). Images on the right show a pen array during the patterning process, highlighting how contact was determined: pens (top) out-of-contact and (bottom) in-contact with the substrate (working electrode) (scale bars = 15 μm) (c) Photograph of the experimental setup in a Park AFM, showing the cell, electrodes, electrical leads, and optical microscope used for leveling.

Controlling Intracellular Machinery via PPL-Based Molecular Patterning

PIs: Mrksich, Mirkin

In another protein patterning approach, **Mirkin** and **Mrksich** used PPL to pattern sub-micron features of fibronectin—an extracellular matrix (ECM) protein—with high aspect ratios and we showed that the orientation of the fibronectin feature can direct the alignment of the actin stress filaments in human mesenchymal stem cells (hMSCs). Fibronectin features were patterned into pre-defined square and circular geometries with unique arrangements and revealed the influence of anisotropy as a cue that directs the assembly of the cytoskeleton and downstream differentiation (**Figure 3**). We learned that the ability to controllably pattern ECM proteins introduces a programmable approach for using sub-cellular spatial cues to control cell behavior within defined geometries. Specifically, we found that human mesenchymal stem cells (hMSCs) grown on a patterned matrix with rounded edges showed preferential differentiation into adipocytes, while patterns that consisted of sharper edges resulted in osteogenesis.[6]

In more recent work building upon this approach, we investigated the ability to program membrane tension by altering the cell shape via PPL patterning in order to tune the degree of endocytosis and exocytosis. We found that cells cultured on patterns with a higher number of external points in the patterns (which generates less tension) had a higher concentration of cholera, as seen by immunofluorescence microscopy and flow cytometry. These results indicate that increasing the tension of the cell membrane decreases endocytosis. We also found that the ligand

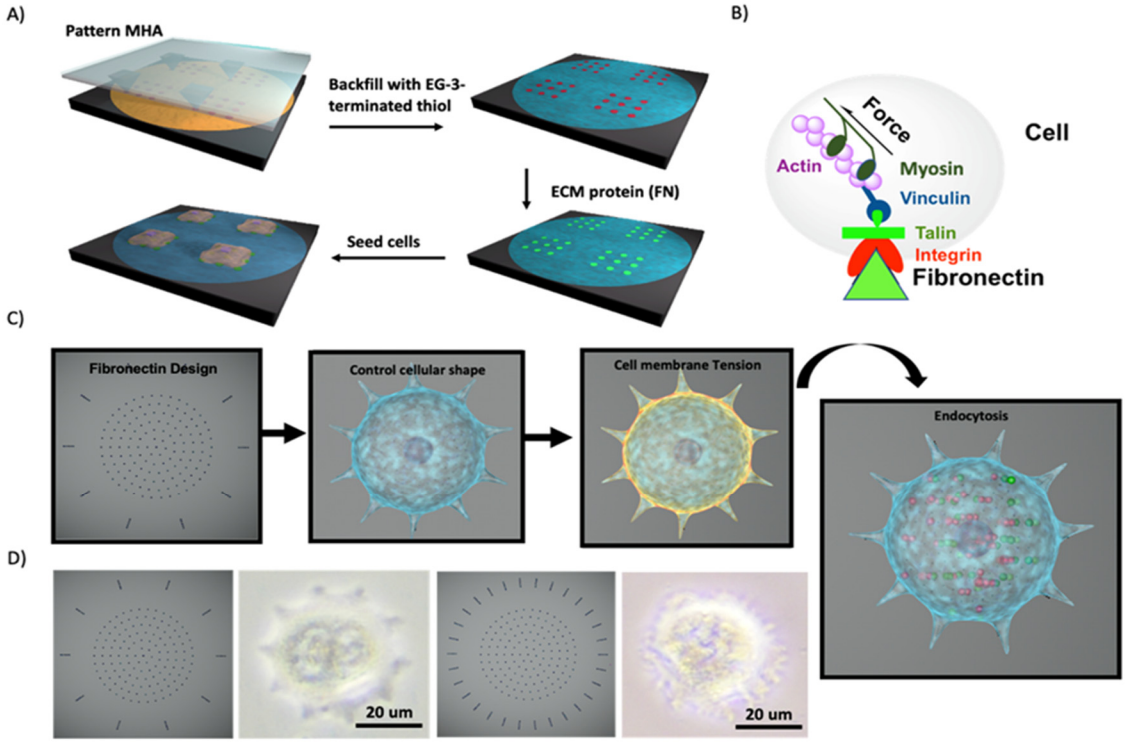

Figure 3. (**A**) Schematic showing the PPL process used to generate extracellular matrix (ECM) protein patterns which were used to seed fibroblast cells. (**B**) Schematic showing the different forces acting on a cell during mechanotransduction. (**C**) Schematic showing how pre-defined fibronectin patterns control cell shape which affects cell membrane tension and ultimately cell endocytosis. (**D**) Confocal images of cells grown on fibronectin patterns where the pre-defined ligand arrangements control cell shape.

arrangements that increase cytoskeletal tension reduce cellular uptake of cholera toxin by regulating endocytic budding. The ability to affect endocytosis by controlling the subcellular spatial cues via PPL is a promising approach to program the cellular endocytic machinery which has implications for creating living devices that monitor how cells respond to extreme conditions or external stimuli.

Development of Cantilever-free Scanning Probes
PIs: Brown, Wang

During the lifetime of the grant the overarching goals of the **Brown** lab were to discover and utilize novel scanning probe architectures to transform the capabilities of cantilever-free scanning probes. At the outset of the program, there were a number of obvious challenges associated with transforming existing nanoprinting techniques into a general purpose 4D nanoprinter. In addition to questions of ink chemistry and integration being addressed by other teams, a major unsolved problem was determining how to make different probes in a massive array write different patterns with materials. Conceptually, the reason for this is that a cantilever-free probe array is based upon a set of probes resting in an array on a compliant film on a rigid backing layer. Since the probes are all co-planar, this limits the ways in which probe-sample contact can differ from probe to probe. This challenge must be overcome to enable general patterning. The prior work in the **Mirkin** group and ongoing work in the **Braunschweig** group has shown that light can be directed onto probe arrays in a spatially coordinated fashion, which can provide a means to independently direct information to each probe, but a means of converting this light into useful motion had to be identified. In the lifetime of this program, we addressed this actuation challenge and, in the process, identified a way to measure the physical state of cantilever-free probes that allows us to use cantilever-free probes for imaging, which is a first of its kind achievement.

The first major contribution during the program was the identification and understanding of photothermal actuation of probes. In collaboration with the **Wang** group who prepared carbon nanotube-elastomer composites, we performed an extensive series of customized experiments designed to measure the motion of an individual probe in response to localized optical illumination. This measurement required the development of a custom atomic force microscope apparatus in which light can be directed through a mask onto a surface that is concurrently interrogated using a scanning probe tip. This system allowed us to address an open question in the community of functional composites. In particular, it was understood that illuminating carbon nanotubes in a polymer matrix can lead to motion, but the nature of this motion was unclear and the subject of debate. Prior work promoted a theory that illumination induced a series of kinks in the tubes that led to an anisotropic contraction. We hypothesized, instead, that the high optical absorption of the nanotubes was leading to local heating which in turn leads to thermal expansion. In order to test this theory and explore the degree to which local illumination could actuate probes, we used the custom atomic force microscope to measure actuation as a function of time, illumination intensity, illumination area, and properties of the film including thickness and carbon nanotube density. By combining these with a finite element analysis-based model of the process, we found that direct photothermal actuation is in good agreement with the observed motion, and thus the kinking hypothesis was inconsistent. With this actuation strategy in hand, the **Wang** group was able to use photoactuation to independently control individual probes.

While our initial successes with photothermal actuation showed the value of this approach, its efficiency and speed required improvement to comprise a suitably scalable actuation strategy. Ultimately, we took three approaches to addressing this challenge. The first leveraged the conceptual understanding we had developed to identify the probe array geometry and illumination conditions that led to the most rapid and efficient actuation. A critical feature of this was the predictive nature of the model we had built of photothermal actuation in carbon-nanotube based composites. The second approach was to micromachine probe arrays to limit the heat conducted between neighboring probes. Physically separating the probes drastically reduced crosstalk effects

between probes and allowed for more efficient actuation. Finally, we explored entirely new strategies of actuation based upon phase-change materials. In particular, by encasing a volatile liquid such as ethanol in a small chamber under each probe, the change in pressure in response to photothermal effects was drastically larger than direct thermal actuation. In sum, these three strategies introduced transformative methods to increase the efficiency and speed of photothermal actuation.

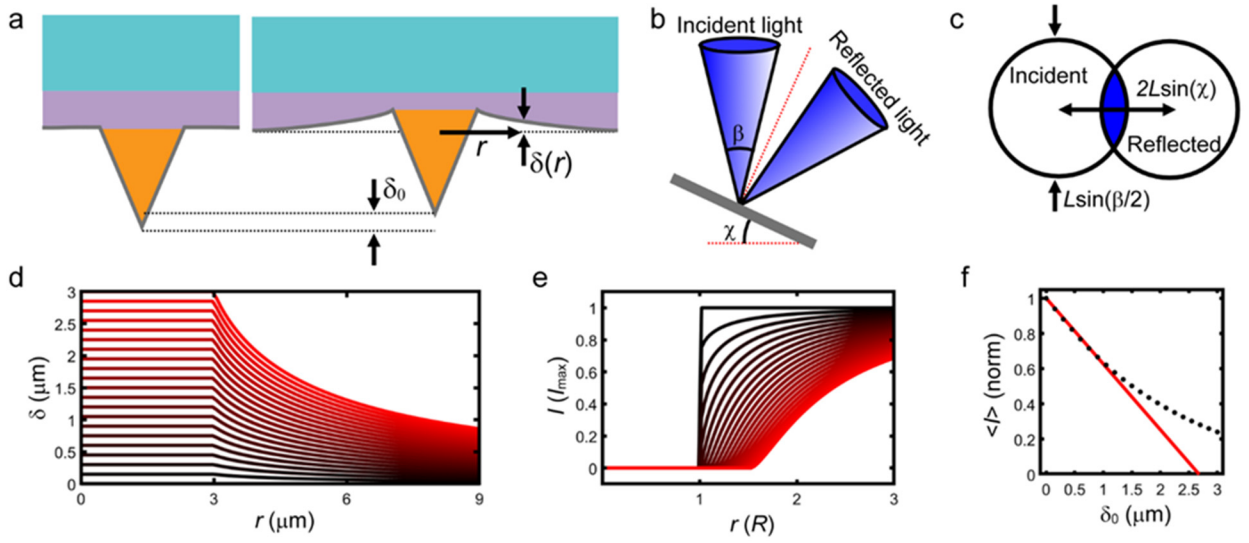

Figure 4. Development and analysis of the distributed optical lever model. (a) Scheme showing a probe being indented a distance δ_0 which leads to the reflective surface at distance r being having a vertical translation $\delta(r)$. (b) Upon rotation by an angle χ, an incident light cone with angular aperture β is reflected. (c) The fraction of the reflected light that is captured is given by the intersection of two circles a distance L from the surface. (d) Calculated δ vs. r profiles with δ_0 varying from 0 (black) to 3 μm (red). (e) Reflected light intensity I normalized by maximum intensity I_{max}. The color scale denotes δ_0 as in (d). The region beneath the probe is assumed to reflect no light due to the sharp nature of the conical probe. (f) Computed area-averaged intensity $\langle I \rangle$ in a 15 μm diameter circle around a probe. The data are well approximated by a line for $\delta_0 \leq 1$ μm with slope 0.37 μm^{-1}.

During the process of addressing the actuation challenge in cantilever-free scanning probe lithography we made several inventions that collectively led to a new paradigm of scanning probe microscopy. This is a fascinating cycle as the original applications of scanning probe lithography, before the cantilever-free architecture, were based upon the atomic force microscope that provided the force-feedback and positioning required to pattern a surface at the nanoscale. Interestingly, completing this cycle and bringing the massively parallel nature of cantilever-free scanning probes to bear on microscopy had not previously been achieved or even conceptualized. Here, the discovery of this new approach began with an advance related to cantilever-based scanning probes. As part of this program, we discovered that one can use direct laser writing (DLW) to directly produce atomic force microscope probes. This provided access to high-speed imaging, a high degree of tunability, and perhaps most importantly, the ability to realize probes on diverse substrates. This led us to hypothesize that such probes could be directly fabricated on compliant surfaces to comprise cantilever-free probe arrays. While such probe arrays could offer more reliable probe-sample contact area, perhaps the more exciting realization was that this could allow for a tighter control of the probe sample mechanics and localize the strain in the backing layer.

The second major innovation we made that led to imaging with cantilever-free probes is that if the probe array is rendered reflective, any deformation of the backing layer is easily optically detected using simple microscopy. Such optical deflection as a signal for mechanical motion is a

well-established idea in cantilever-based probe microscopy where the cantilever serves as an optical lever that redirects a beam of light upon bending. Thus, we termed our invention the 'distributed optical lever' in that it performs the same function but does not require a cantilever (**Figure 4**). We determined that this approach can easily achieve single digit nanometer vertical resolution, close to the value obtained by state-of-the-art probe microscopy. However, instead of requiring a delicate and difficult to produce cantilever, the cantilever-free probes can be realized and measured in massive arrays. As a demonstration of this, we produce an array of over 1000 probes that can be independently observed. We then developed a process for moving the probe array along a surface, imaging the surface, and then reconstructing the resulting images into a topographical image that spans over fifty times the maximum area of a conventional atomic force microscope. In addition to reporting this first-of-its-kind strategy for massively parallel imaging which will have implications for the metrology community generally, the use of this technique in conjunction with 4D nanoprinting will allow us to address questions of registration, pattern fidelity, and quality that were previously impossible to address.

In summary, the **Brown** group led the development of a series of novel patterning and imaging techniques centered around cantilever-free probes that collectively transform their capabilities. Specifically, the main advances were in the area of independently addressing individual probes and then reporting the probe-sample contact in a manner that provide real time topographical information. These advances dovetail well with the work from the other teams on developing novel ink formulations and integrating these architectural and technique advances into robust printing strategies.

Photoactuated Pens for Molecular Printing

PIs: Wang, Brown, Mirkin

Control over each individual pen during polymer pen lithography (PPL) is needed to create complex large area patterns but is extremely challenging since there can be millions of these nanoscale pens in a single array. One solution is photoactuated PPL (pPPL), which uses site-specific irradiation to physically move individual pens through changes in material strain (**Figure 5C**).[7] A polymer-carbon nanotube composite was identified as a suitable light-responsive material that the pen arrays can be made from. Irradiation causes the pens to extend by up to 3 μm, enabling selective patterning using only the pens that are irradiated. This photoactuation could be controlled over 16 pens at once, a significant improvement over using the thousands to millions of pens simultaneously in a typical pen array. Deploying more precise illumination sources will provide control over a single pen at a time.

Dynamic actuation of individual pens in a massive pen array is an ambitious goal for nanomanufacturing and an important step to realize patterning and printing of molecules at high-resolution and low-cost. **Wang** designed and fabricated PDMS-CNT composite pens and showed for the first time that it is possible to photo-actuate the microfabricated polymer pens for molecular printing. **Wang** and **Brown** further collaborated to reveal the photothermal dynamics and mechanism underlying the photoactuation.[7-9] For precise and effective photoactuation, we find it is important to achieve uniform dispersion of CNTs in the polymer matrix. We addressed this challenge by grafting alkyl chains ($-(CH_2)_5CH_3$) that significantly enhanced the solubility of CNTs in the same solvent for PDMS. **Figure 5** shows the pen array fabricated on a 4 cm × 4 cm superflat glass slide and the photoactuated patterning by one of the pens when light is on and off. Based on this work, **Wang** and **Brown**, in collaboration with **Mirkin** and **TERA-print**, LLC have made crucial progress on enhancing actuation efficiency and reducing crosstalk, via the innovation of pen architecture and the inclusion of thermal insulating light absorber. We successfully demonstrated the capability of photoactuating the pen array at a resolution as high as just 3x3 pens. Our experiments demonstrated that the photoactuated expansion is significant enough to control the writing behavior of the pens with an illumination area of 170 μm x 170 μm.

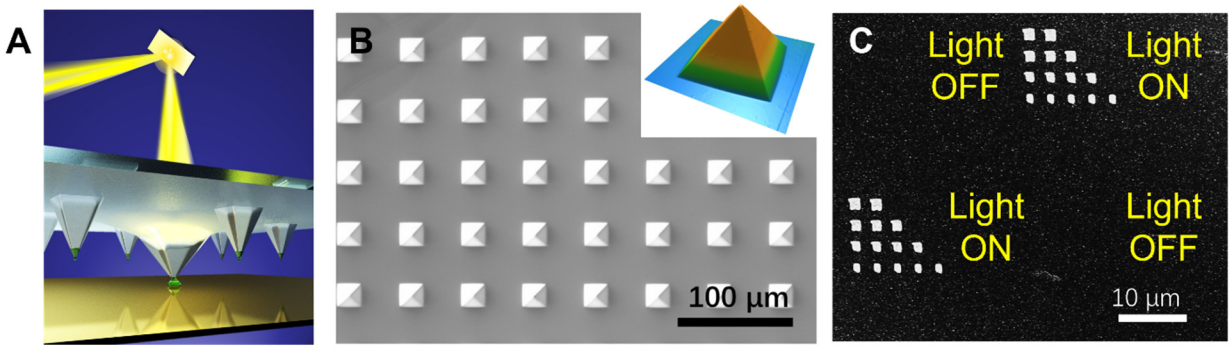

Figure 5. Photo-actuated CNT-PDMS pen arrays. (A) Schematic of photoactuated molecular printing. (B) Scanning electron microscopy (SEM) image of a section of the CNT-PDMS pen arrays. Inset is 3D AFM image of the pyramidal tip. (c) SEM of etched gold patterns written by a pen at different levels of photoactuation.

Wang has also collaborated with Dr. Bryan **Glaz**'s group in the **U.S. Army Research Laboratory** on the investigation of the mechanical properties of light responsive composites. Together we have demonstrated the use of ultraviolet light and a photoreactive molecule, benzophenone, to control the interfacial adhesion between CNTs and PDMS matrix. By triggering interfacial bonding chemistry with light, we show the elastic modulus of the PDMS-CNT composite can be increased in situ by as much as 93%.

4-Dimensional Polymer Brush Patterns with a Photochemical Printer
PI: Braunschweig

A primary aim for the MURI award was to create patterns where the position (*x*, *y*), height (*z*), and chemical composition of molecules in a pattern can be controlled independently for each sub-1 μm^3 voxel in a pattern. We refer to such structures as 'polymer brush hypersurfaces' and not '3D prints' or '3D structures' because the three cartesian dimensions are not sufficient to define their

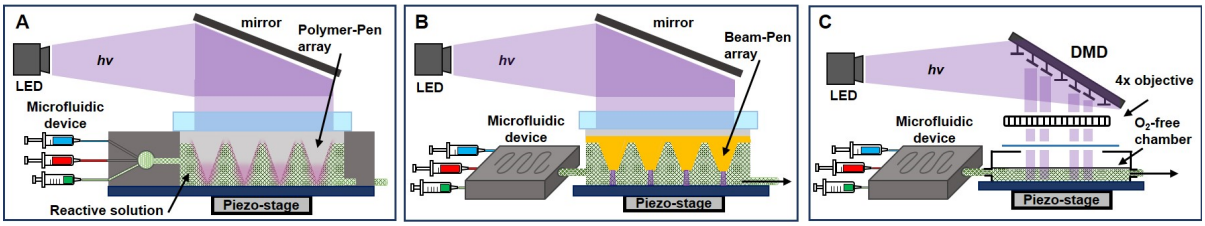

Figure 6. Systematic Development of Hypersurface Photolithography. (A) Integration of a light source, fluid cell, and polymer pen arrays to carry out photochemical reactions on a surface. (B) Addition of sophisticated microfluidics for improved ink mixing and inclusion of beam pen arrays (BPAs) for smaller features. (C) Incorporation of a digital micromirror device for individual pixel actuation and a reaction chamber for carrying out oxygen-sensitive reactions.

structure. For example, defining any voxel in a block copolymer hypersurfaces would require at least 4 orthogonal dimensions – (i and ii) *x, y* position across the surface, (iii) height, *z*, and (iv) chemical composition. Rather than refer to these objects as '4D prints', '4D structures', or '4D surfaces', we use the term hypersurface because '4D printing' has already been coopted by the printing community to refer to objects whose structures change with time, and to also recognize that these polymer brush patterns may necessitate more than 4 variables for a complete description. Printing hypersurfaces required overcoming major limitations in printer design, and to this end Braunschweig group has created a hypersurface printer by systematically testing and optimizing new printing ideas that integrate massively parallel scanning probe arrays, fluid cells, light sources, and surface chemistries (**Figure 6).** First, we designed a massively parallel photochemical microreactor that integrates PPL arrays within a PDMS flow-through fluid cell (**Figure 6A**), where photochemical organic reactions occur in solution rather than within a polymer matrix. In this device, reagents can be introduced successively into the reaction chamber, allowing the printing of inks of different composition in close proximity (< 5 μm). In the next step we combined microfluidics, beam pen lithography (BPL), and photochemical surface reactions to create multiplexed arrays (**Figure 6B**). In this printer, we demonstrated three important innovations that, taken together, enable versatile printing of multiplexed patterns by tip-based lithography. Specifically, these are that (1) the polymer pen arrays are replaced with beam pen arrays, which focus light and significantly reduce the background signal, (2) the fluid cell is removed, and instead reactions occur within a droplet pulled below the array by capillary forces, and (3) reactant solutions are mixed in a microfluidic cell upstream of the droplet, enabling the efficient switching of inks. Finally, we report a new hypersurface printer (**Figure 6C**), where the monomer composition and feature height of each pixel in a large (>1 cm^2) polymer brush pattern can be controlled independently and with ~5 μm pixel edge-length. To create these 4D prints, we integrated a digital micromirror device with 1024 x 768 independently controllable mirrors, microfluidics, and an oxygen-free reaction chamber with a CPU interface to project patterns from an image file onto the substrate.

Fabrication of Polymer Thin Films for Beam Pen Selective Self-Assembly
PIs: Gianneschi, Mirkin

The ability to construct polymeric three-dimensional architectures is attractive for applications in catalysis, electronics, biosensing, and bio-functionalized surfaces. However, constructing well-defined architectures is limited by spatiotemporal control over the resulting assembly. With the onset of beam pen lithography (BPL), photoactivation of polymeric "inks" for control over the assembly have been explored. Self-assembling, peptide progelators have proven a robust model to construct architectures with spatiotemporal controls **(Figure 7)**. Cyclic progelators were previously investigated as an attractive biomaterial for the application of photopatterning. Through the alternation of charged and hydrophobic groups, gelation of linear peptides into an entanglement of beta-sheet fibrils has been shown. In cyclic conformation, sterically constrained cyclic progelators exhibit low viscosity effects. By incorporating a UV responsive moiety within the cyclic backbone, we hypothesized local cleavage, linearization, and beta-sheet assembly of

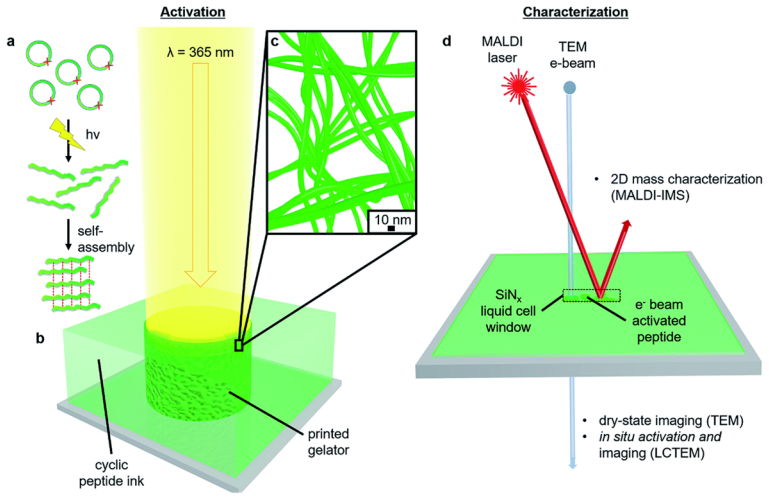

Figure 7. Schematic of UV-responsive ink activation and characterization. (a) Sterically constrained cyclic peptide linearizes in response to UV activation and self-assemble through amphiphilic interactions. (b) Bulk scale activation from a solution of cyclic peptide ink provides a means for 4D printing of an ECM-like gel comprised of (c) entangled nanofiber networks. (d) Characterization of silicon nitride (SiN_x) chip surfaces to explore morphology by transmission electron microscopy (TEM) and chemical signatures by matrix-assisted laser desorption ionization imaging mass spectrometry (MALDI-IMS).

progelators through UV patterning.

With this hypothesis, we developed charge conversion progelators, which self-assemble through local reducing environmental conditions. The positively charged moieties are acid capped to force the net charge of the peptide's isoelectric point to be negative, which effectively increases solubility of the linear progelator. To develop a system amenable to beam pen lithography, we made polyacrylamide hydrogels dispersed with charge conversion progelators and photoacid generators to locally activate self-assembly and gelation. This study validates our hypothesis for conformational steric hindrance as a method of activating a bioink and we demonstrated that with UV activation, bulk scale, and localized self-assembly, respectively, were possible, with predictable cleavage products.

In-situ Observation of PAE Superlattice Formation Using Liquid-cell TEM
PIs: Mirkin, Gianneschi

Liquid-cell transmission electron microscopy (LC-TEM) is a high-resolution analytical technique that allows samples to be imaged in their native liquid environment. This environment maintains the dynamic nature of nanoscale assemblies and provides a means to interrogate their kinetics and crystallization pathways. This is accomplished by confining a thin layer of liquid between two substrates with electron-transparent windows for sample analysis. We have

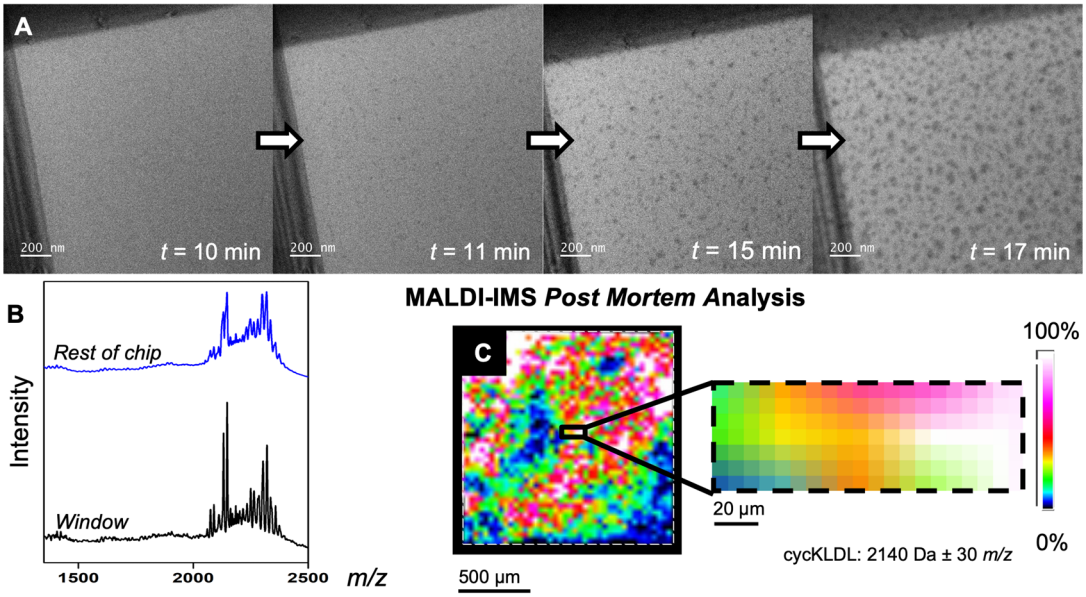

Figure 8. TCEP activation of cycKLDL to form nanoscale structures in situ. **A**. LCTEM images of a solution of cycKLDL and TCEP acquired under low-flux, pulsed conditions. **e** Top right corner of the same liquid cell, which had not been previously irradiated. **B.** Overall mass spectra of liquid-cell chip. **C.** MALDI-IMS mapping of chip from the LCTEM experiment shown with a 2140 ± 30*m/z* mass filter.

developed and optimized new liquid-cell architectures that are electron-transparent (using silicon nitride windows), resist electron beam-induced damage to samples (using graphene oxide layers) and maintain the structure of preassembled colloidal crystals (using dehydration-rehydration cycles). We have explored 'post-mortem' verification to understand how the assembly of the liquid cell affects the superlattice structure and have demonstrated that nanoparticles remain mobile in the liquid cell. We have deployed these advances to start to address questions about nucleation-growth mechanisms in colloidal crystallization and the emergence of order in thermally-annealed superlattice samples.

Liquid-cell transmission electron microscopy (LCTEM) is an in-situ imaging technique for imaging solvated nanomaterials in real time, was leveraged to observe stimuli-induced peptide-based nanoscale assemblies. Despite broad interest in characterizing biological phenomena via LCTEM, electron beam-induced damage remains a significant problem. Moreover, methods for verifying chemical structure during or following an LCTEM experiment have been few, with key examples limited to electron diffraction or elemental analysis of crystalline materials, a strategy not translatable to biopolymers observed in nature. In a proof-of-concept study, the **Gianneschi** group leveraged LCTEM with matrix-assisted laser/desorption imaging mass (MALDI-IMS) as a post-mortem correlative mass spectral technique.

This powerful multimodal strategy was used to study oligomeric peptide nano-assemblies, which were triggered by biological or chemical stimulants via LCTEM. This approach confirmed whether higher-order assemblies observed by LCTEM consisted of intact peptides, verifying that observations made during the in-situ experiment are because of those same peptides and not aberrant electron beam damage effects (**Figure 8**).

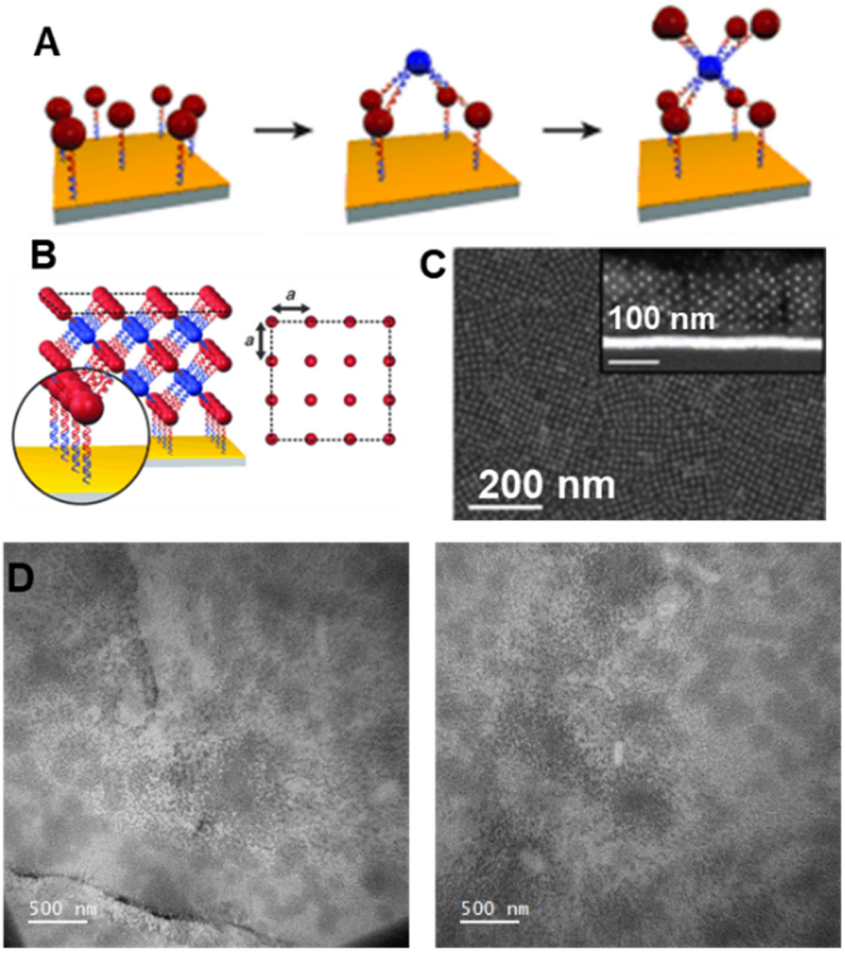

Figure 9. LCTEM studies of PAEs. **a.** Fabrication protocol of PAEs on SiNx. **b.** Side view of assembled PAEs. **c.** SEM micrograph of annealed PAE lattice. **d.** LCTEM micrographs of heated, hydrated PAE.

Efforts were also made in collaboration with the Mirkin group to observe and modulate the assembly of programmable atom equivalents (PAEs) (**Figure 9**). These PAEs are formed by functionalizing the SiNx substrate with complementary strands of nucleic acids and high contrast gold nanoparticle markers will anneal at precise temperatures, both as a function of heating rate and strand composition. These systems were investigated using VT-LCTEM to observe the annealing and crystallization process. However, anomalous interactions between the electron beam and the nanoparticles, further exacerbated by the high degree of spatial confinement in the liquid cell environment, have occluded this process from successful observation. The lattices have been successfully observed at high resolution in a hydrated environment but have remained static or damaged in the viewing area over the course of experiments.

Macroscale High-Area Rapid Printing in 3D
PI: Mirkin

Additive manufacturing has been transformative in the fields of design and manufacturing. We have developed an approach known as HARP (high-area rapid printing) capable of printing over large areas at rapid vertical printing speeds (**Figure 10 and 11**).[3] HARP operates through a mobile liquid interface which creates a shear stress beneath the emerging part and results in a slip boundary. The slip boundary allows for the solidified part to be continuously retracted from the print interface. A pair of inlet and outlet manifolds were fabricated to distribute a laminar flow of oil across the print-bed with a uniform velocity profile. This flow profile ensures that the oil layer remains optically uniform across the build platform (*i.e.*, no turbulence giving rise to optical distortions at the oil/resin interface) and results in the application of a uniform interfacial-shear stress to all solidified parts. We hypothesized that that a slip-boundary is vital to our printer's operation.

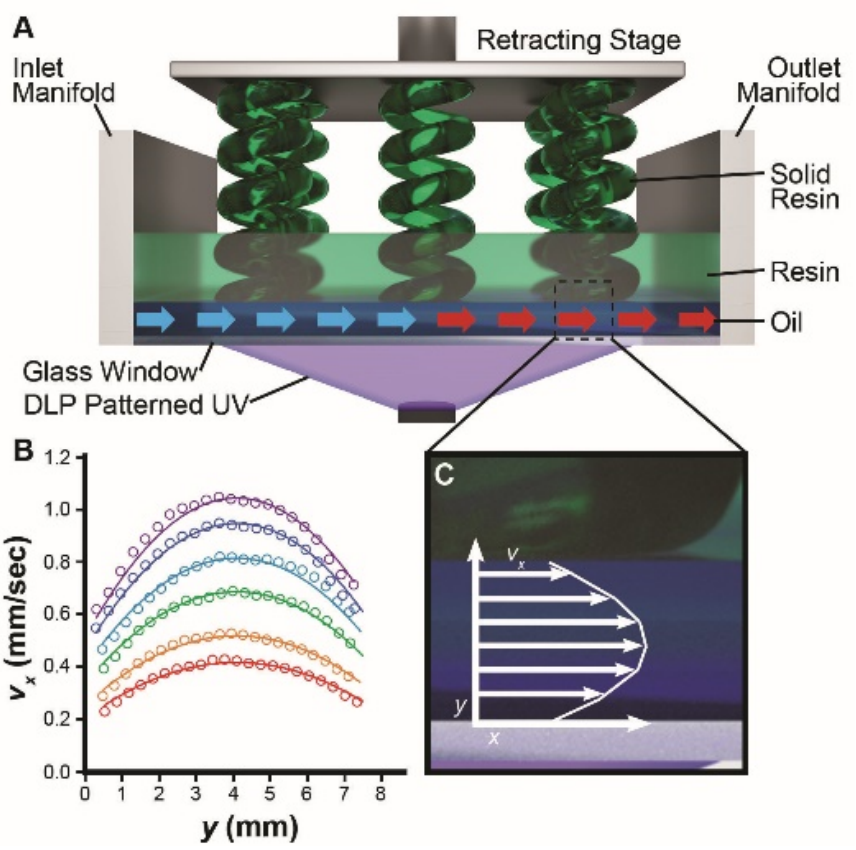

Figure 10. Flow profile of a mobile interface that enables continuous printing. **(A)** Scheme of a 3D printed part emerging from the HARP 3D printer. **(B)** Velocity profile under the printed part at different flow speeds demonstrating the presence of a slip boundary (colors represent increasing volumetric fluxes, *q; red* is q = 0.21 mm/s, *orange* is q = 0.30 mm/s, *green* is q = 0.44 mm/s, *teal* is q = 0.56 mm/s, *blue* is q = 0.66 mm/s, *violet* is q = 0.75 mm/s; open markers are experimental data points from particle imaging velocimetry; continuous lines are fits from an analytical model). **(C)** Scheme of the slip-boundary flow profile under the part with a representative experimentally observed flow profile depicted.

To test this, we used particle imaging velocimetry to analyze the cross-sectional fluid-flow profile as the oil passed beneath a printed part. An analytical model, allowing for the possibility

of either a slip or non-slip boundary condition, was fit to the center of the flow-profile. From this analysis, the slip-boundary model best captured the dynamics of the experimental data (**Figure 10B**). This is best reflected in the experimental velocity profiles (vx(y), open markers, **Figure 10B**) as a function of the oil flow rate (increasing volumetric flux, from red to violet) and the corresponding Navier slip model fits (solids lines, **Figure 10B**).

The key innovation of HARP over comparable stereolithographic methods is that HARP eliminates the 'dead layer' inherent in other techniques. The highly exothermic polymerizations used in patterned resins are cooled using an immiscible oil to overcome the challenge of heat dissipation that plagues other rapid printing techniques. The oil layer can be recirculated to continuously control the cooling temperature and filtered to remove any solid micro-particulates generated during the printing process. Furthermore, because this approach does not utilize an oxygen 'dead-layer,' it is compatible with oxygen-sensitive resins, increasing the available ink chemistries and the scope of compatible materials. These advances in throughput, mobile interface design, and material generality solve several of the problems often associated with large area and large object 3D printing.

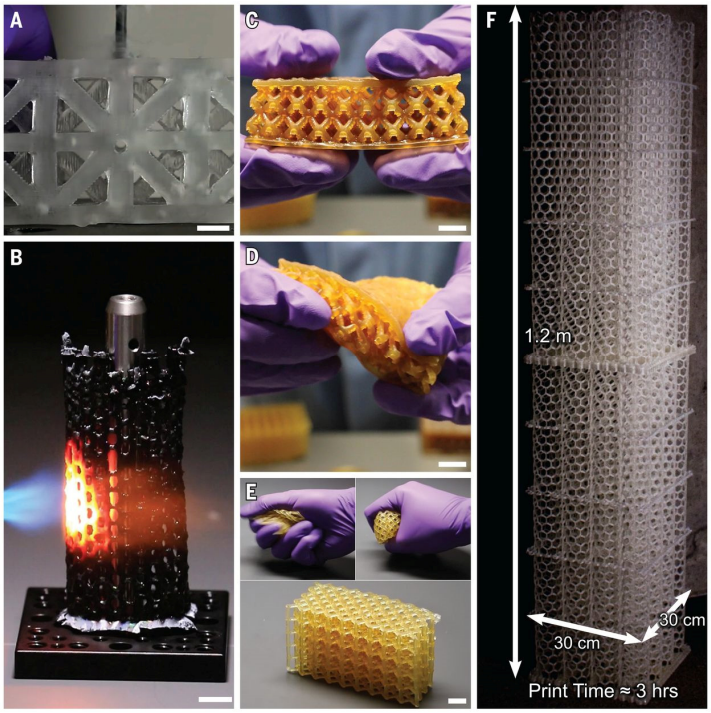

Figure 11. (**A**) A hard, machinable polyurethane acrylate part (print rate, 120 μm/s; optical resolution, 100 μm) with a hole drilled against the print direction. Traditional noncontinuous layer-by-layer printing techniques typically delaminate and fracture when drilled in this orientation. (**B**) A post-treated silicon carbide ceramic printed lattice (print rate of green polymer precursor, 120 μm/s; optical resolution, 100 μm) stands up to a propane torch (~2000°C). (**C** and **D**) A printed butadiene rubber structure (print rate, 30 μm/s; optical resolution, 100 μm) in a relaxed state (C) and under tension (D). (**E**) Polybutadiene rubber (print rate, 30 μm/s; optical resolution, 100 μm) returns to expanded lattice after compression. (**F**) A ~1.2-m hard polyurethane acrylate lattice printed in less than 3 hours (vertical print rate, 120 μm/s; optical resolution, 250 μm). Scale bars, 1 cm.

TA2: Synergistic Efforts for Ink Chemistry

Novel Ink Compositions
PI: Mirkin

We have greatly expanded on BPL capabilities and applications by developing inks with a variety of functional properties. Nanoparticle superlattices containing up to three different components have been patterned using BPL, enabling the formation of unique colloidal crystal structures. Photo-responsive hydrogels were patterned using BPL to create synthetic extracellular matrices with programmable stiffness, length, size, and density (**Figure 12**).[6] This control over

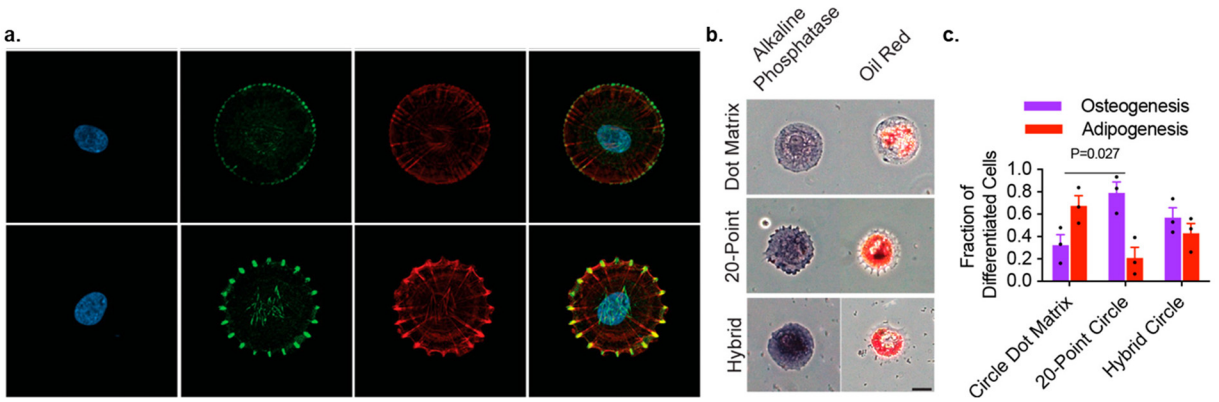

Figure 12. (**a**) Fluorescence micrographs of the focal adhesions and actin cytoskeleton within cells on BPL patterns. Representative confocal images of single cells grown on different patterns: dot matrix circles (top) and 20-point circles (bottom). The nucleus (panel 1), focal adhesions (vinculin, panel 2), and actin cytoskeleton (panel 3) are labeled within each cell. Panel 4 shows the overlay of the different structures. (**b**) Bright-field images of cells on each respective pattern strongly staining purple as an osteogenic marker (left column) or red as an adipogenic marker (right column). Scale bar: 25 μm. (**c**) Percentage of cells staining positive for only adipogenic or osteogenic markers (mean ± SEM; $p = 0.027$; one-way ANOVA with Tukey's honestly significant difference *post hoc*), indicating stem cell differentiations.

hydrogel structure enabled us to study how the physical properties of the ECM dictate cellular behaviors (*i.e.*, cell migration and differentiation). Furthermore, a new type of protein ink based on protein 'megamolecules' was developed and used to bind specific cellular targets and even effectively deliver drugs to cells.[10] This ink will be applied toward BPL patterning of bioactive molecules. Additionally, a responsive BPL ink was developed that enables the rapid gelation of patterns with predetermined stiffnesses in response to specific stimuli. These advancements allow for new BPL capabilities in a wide variety of fields.

Protein Capture and Patterning using Photo-Active Inks
PI: Mrksich

The **Mrksich** laboratory made several advances in the patterning of bioinks with lithographic and optical techniques and also in the development of megamolecule-based bioinks with complex architectures. In one of the early research publications, we described how proteins can be patterned via surface reactions on self-assembled monolayers with high fidelity and high resolution, with patterning features achieved at the nanoscale (**Figure 13**).[11] We showed that proteins and

megamolecules containing the enzyme SnapTag can be captured on monolayers presenting a SnapTag capture ligand that forms a covalent bond with SnapTag. Furthermore, we showed that we can photoprotect the SnapTag capture ligand and use photomasks to deprotect the capture ligand with ultraviolet light, then expose the surface to SnapTag-containing proteins to achieve nanoscale patterning. Sequential deprotection and capture steps enabled patterned immobilization of two proteins. We demonstrated that SnapTag-fused antibodies specific to cell surface receptors can be immobilized with this method, enabling the selective capture and patterning of cells expressing the target proteins. This work demonstrated a chemisorption approach to patterning proteins that was directly compatible with immobilization of more complex protein-based megamolecules, as SnapTag is frequently used in the megamolecule assembly process. The ability to direct covalent protein immobilization with light will allow for sub-diffraction-limited patterning, potentially enabling patterning at the single protein length scale. Furthermore, we reviewed the scientific progress of dynamic substrates for cell biology, describing the strategies to manipulate ligand activity, highlighting recent work that has advanced the field.[12]

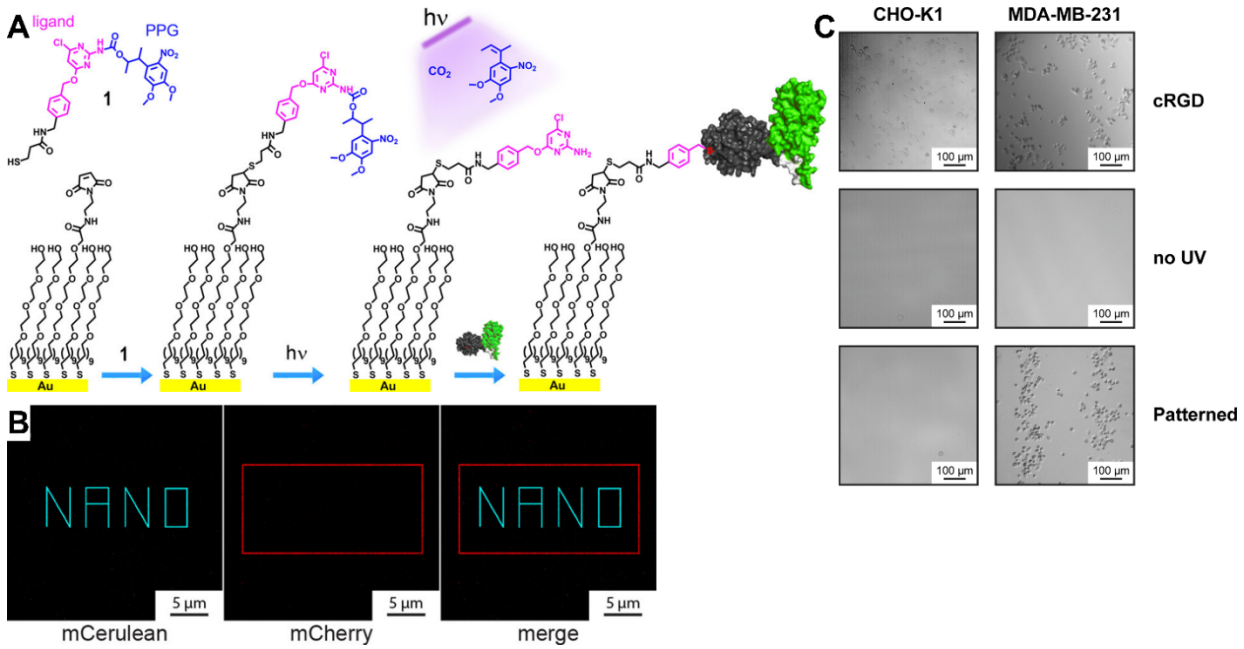

Figure 13. Schematic and results of photopatterning of proteins. (**A)** Protein coupling to **1** is blocked by a nitrophenyl photoprotecting group (PPG). The surface was prepared by self-assembly of a maleimide-presenting alkanethiolate monolayer. Then, **1** was immobilized to the surface. Next, the photoprotecting group was removed by UV illumination. The SnapTag fusion protein was covalently bound to illuminated regions. (**B)** Fluorescence micrographs of a surface patterned with two proteins. Sequential illumination and capture of mCerulean-SnapTag and mCherry-SnapTag using a focused laser on a microscope. (Left) mCerulean (blue) channel showing a pattern of the word "NANO". (Middle) mCherry (red) channel showing a rectangular pattern. (Right) Merged image of the two channels shows colocalization of the two patterned fluorescent proteins. (**C)** Bright-field micrographs of cell lines cultured on patterned surfaces. Two different cell lines, CHO-K1 (CEA–) and MDA-MB-231 (CEA+), were grown for 6 h on surfaces that present cyclic RGD (cRGD), the photoprotected ligand (**1**) incubated with anti-CEA scFv-SnapTag (no UV), and the photopatterned ligand (**1**) incubated with anti-CEA scFv-SnapTag (patterned).

We discovered an interesting case where surface reaction kinetics on a self-assembled monolayer differed significantly from solution.[13] The second-order rate constant for this surface reaction was approximately 100-fold greater than that for the analogous solution-phase reaction.

This work provided a well-characterized example that illustrated the extent to which the kinetics and properties of an interfacial reaction can depart substantially from their solution-phase counterparts.

Development of BioInk Chemistries using the Megamolecule Platform
PI: Mrksich

We have made several significant advances in our ability to generate complex bioinks using the megamolecule platform. These structures are composed of proteins that are crosslinked using enzyme promoted reactions to created large, covalent protein structures that can be massive (> 500 kDa; > 50 nm), take on a variety of superstuctures (linear, branched, cyclic, dendritic) and are structurally perfectly defined. A key advantage of bioactive inks is that wide varieties of protein function are incorporated into inks, enabling printing of enzymes, antibodies, fluorescent proteins, and other activities. We synthesized several new fluorescent bioinks, where a fluorescent protein is fused to SnapTag, creating a fusion protein that incorporates both a fluorescent domain (*i.e.*, the fluorescent protein) and a surface attachment domain (*i.e.*, SnapTag). The fluorescent inks serve three purposes—1) they can be visualized by fluorescence microscopy and are spectrally resolvable, 2) multicolor megamolecule inks can be created from simple protein inks through the megamolecule bioconjugation strategy developed by the Mrksich lab, and 3) fluorescent inks serve as a surrogate ink for functional bioinks that cannot be visualized microscopically (*e.g.*, antibody-containing inks). In one publication, in order to understand the size of megamolecule inks in solution, we measured energy transfer in megamolecule inks to serve as a molecular ruler.[14, 15] These inks were multicolor, which represented our first example of multifunctional bioinks. Donor and acceptor fluorescent protein molecules were incorporated into large, megamolecule protein structures. We observed fluorescence resonance energy transfer in protein megamolecules across long distances (>10 nm). The efficiency and rate of energy transfer is distance-dependent, and even large and long megamolecules exhibit energy transfer (*i.e.*, trimer conjugates exhibit energy transfer).

To further gain control over the relative placement of multiple protein domains at the nanoscale, we synthesized megamolecules composed of four arms (**Figure 14**).[16] This was made possible through synthesis of new tetravalent linkers, with the added functionality of metal ion chelation which is valuable in many applications. We synthesized tetravalent linkers with three different lengths of spacers between the core and the protein attachment site and rigorously studied the resulting megamolecules by ESI-MS, TEM and X-ray crystallography. We learned the constraints of generating four-armed structures and how to tune their design with nm-scale resolution.

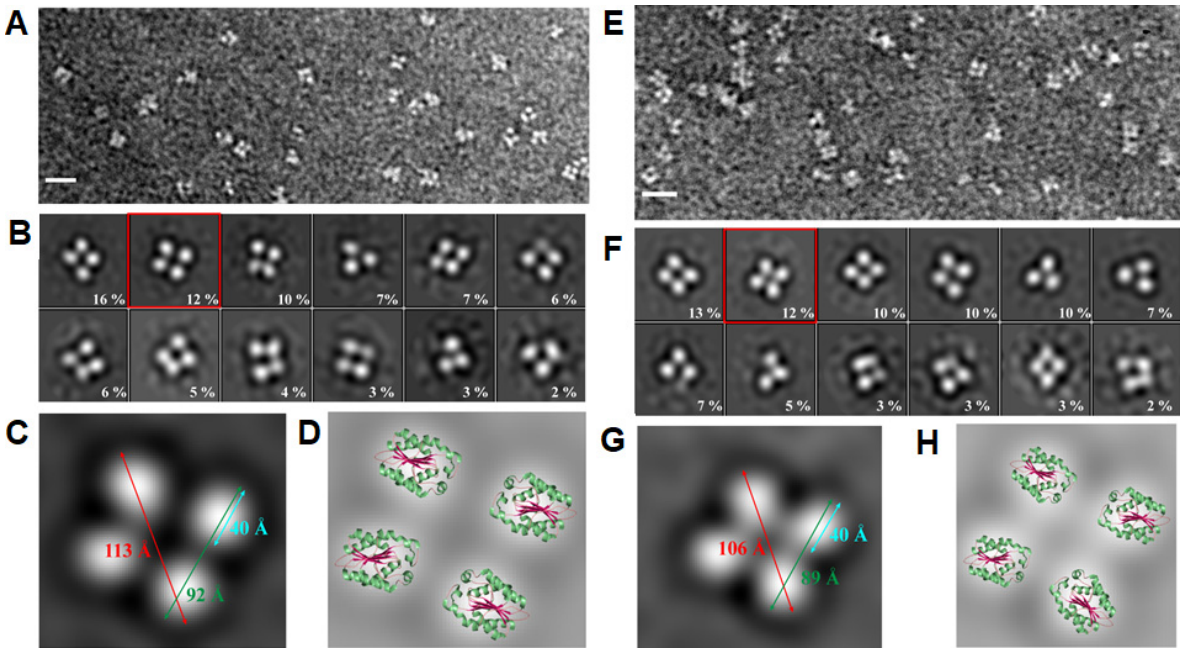

Figure 14. Negative stain TEM shows the structure of the four-armed megamolecules. (**a**) Representative TEM image of negatively stained $(Cut)_4$-L molecule. Scale bar represents 20 nm. (**b**) Reference free 2D class averages of all the particles picked from the micrographs of $(Cut)_4$-L. Percentage of particles in each class is noted. (**c**) Measured dimensions of one of the classes (red box in **b**, fully extended top view) of the $(Cut)_4$-L molecule. (**d**) Coordinates of four Cutinase molecules (PDB ID: 1CEX) overlaid on the 2D average to represent the structure of the $(Cut)_4$-L molecule. (**e-h**) The same TEM characterization and analysis corresponding to **a, b, c,** and **d** for $(Cut)_4$-M. The class of $(Cut)_4$-M used to measure its dimensions (red box in **f**, fully extended top view).

Toward understanding the precise placement and behavior of enzymes, we studied the effect of immobilization of a single enzyme in a three-dimensional architecture on catalysis. In collaboration with the **Hupp** and **Farha** groups at Northwestern University, the **Mrksich** group studied the effect of encapsulation on the activity of cutinase, an enzyme used in the production of megamolecule ink.[17] This study highlighted the ability of enzymes to retain activity after immobilization in a metal-organic framework three-dimensional structure, providing further evidence that protein-based megamolecule inks could be catalytically active after 3D printing. Further, this proof-of-concept study revealed increased stability of the enzyme to denaturants, suggesting that 4D materials printed with megamolecule ink will feature improved enzyme stability, relative to free enzyme.

In another example, we generated multifunctional bioinks, containing combinations of fluorescent proteins, affinity domains for cell-surface proteins, and desirable enzyme activities.[18] We varied the relative number of nanobody affinity domains and enzymes and studied their impact on cell binding and enzyme activity. We determined the Michaelis-Menten parameters of variants and saw the largest catalytic efficiency (k_{cat}/K_M) in structures with two enzyme copies and the smallest catalytic efficiency in the versions with one enzyme copy. The relative rates suggested that intramolecular dimerization (where dimerization is required for this enzyme to be active) was responsible for the increased enzyme activity. Further, we quantified megamolecule molecular recognition on cells. We observed that binding was specific to cells expressing the target protein, and observed that megamolecules with two affinity domains bound to the target cells with greater affinity. This work was recently published, incorporating additional work conducted in this reporting period, described in greater in Part II.[19]

Development of Photoactive Inks for Fabrication of 2D/3D Functional Polymeric Materials
PIs: Mirkin, Gianneschi, Braunschweig

Over the past several years, significant progress has been made toward expanding the capabilities of BPL, specifically in the development of new, photo-active inks. The development of hierarchical ink chemistries is important to advancing the printing of functional architectures. Toward this goal, we explored the integration of biologically active molecules, including oligonucleotides and proteins, into inks containing light-reactive molecules. A light-responsive small molecule was incorporated into the gelling sequence of a self-assembling, cyclic peptide progelator, which could then be patterned on a surface using BPL. When stimulated with UV light, the peptide cleaves to become linear, which forms entangled secondary and tertiary structures and dictates the mechanical properties of the material. Additionally, photoactive polymer-peptide conjugates were developed toward the goal of making light-triggered 3D printed materials for controlling material properties such as cell adhesion. Model studies were conducted using photo-RAFT between two different peptide sequences and an acrylamide small molecule to make peptide brush polymers. These polymerizations were also shown to work in aqueous solvents in addition to organic solvents. Finally, we also developed a light-driven chemistry for covalently coupling functional groups to carbon nanotube thin-film substrates. Small molecules could be attached to the nanotube surface by exciting distinct locations on the surface with laser irradiation with feature sizes of 1 μm. This work has developed a strong foundation that will allow us to pursue applications in oligonucleotide array synthesis, protein immobilization, biosensing, and photonic devices.

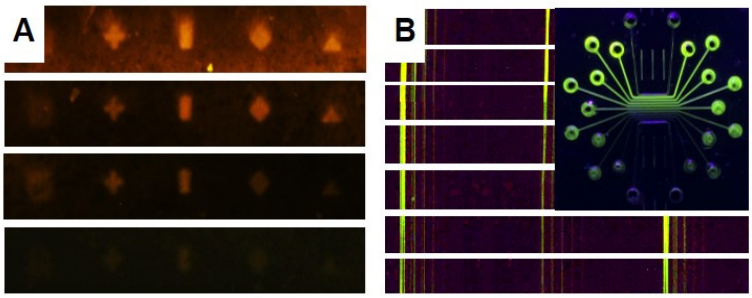

Figure 15. Application of Hypersurface Photolithography. (A) Multiplexed array with five alkene-labeled glycans. (B) Fluorescence image of Man-5-containing brushes of varying heights patterned into vertical lines after exposure to FITC-ConA. Inset is a fluorescence image of the incubation chip containing FITC-ConA solutions at 9 different concentrations.

The **Braunschweig** group developed new photochemical surface reactions to create functional hypersurfaces. To demonstrate the capabilities of these new surface-initiated photochemistries we have created glycan microarrays and stimuli-responsive polymer brush hypersurfaces. To develop our glycan-array capabilities, we first printed a multiplexed glycan microarray where different glycans were printed onto the same surface using thiol-ene photoreactions to study lectin binding (**Figure 15A**), and we found that natural binding trends and selectivities could be reproduced. The density of α-Mannose was then varied systematically to explore the relationship between surface valency and cooperativity on lectin binding. Building upon the knowledge gained, a glycopolymer microarray was fabricated by combining ethylene glycol dimethacrylate, pentaerythritol tetrakis(3-mercaptopropionate), and alkene-labeled mannose to create a copolymer brush, which binds the mannose-specific glycan binding protein, concanavalin A (ConA), with sub-femtomolar avidity (**Figure 15B**), which is the most sensitive glycan microarray yet developed. In addition, the

versatility of the chemistry and the hypersurface printer allowed us to explore the binding between the glycopolymers and ConA, and we found that binding proceeds with negative cooperativity. These results open many new opportunities in glycobiology, where ultrasensitive detection of glycan-binding with these surfaces will provide the unprecedented ability to investigate the complex role of carbohydrates in biology.

MALDI-IMS of polymer brushes patterned on surfaces

PIs: Gianneschi, Braunschweig

In 2018, we reported on the development of matrix-assisted laser desorption/ionization imaging mass spectrometry (MALDI-IMS) as a sensitive and nondestructive technique that possesses the high spatial resolution and precision necessary to produce a 2D map of photopatterned poly(methyl methacrylate) (PMMA) surfaces. The **Gianneschi** and **Braunschweig** groups leveraged MALDI-IMS to characterize surface-bound polymethacrylate. The surface polymers were prepared via a technique termed Polymer Brush Hypersurface Photolithography, which produces polymeric pixels by combining a digital micromirror device (DMD), an air-free reaction chamber, and microfluidics to independently control monomer composition and polymer height of each pixel. This approach accelerates reaction discovery and enables rapid optimization of polymer coatings (**Figure 16**).

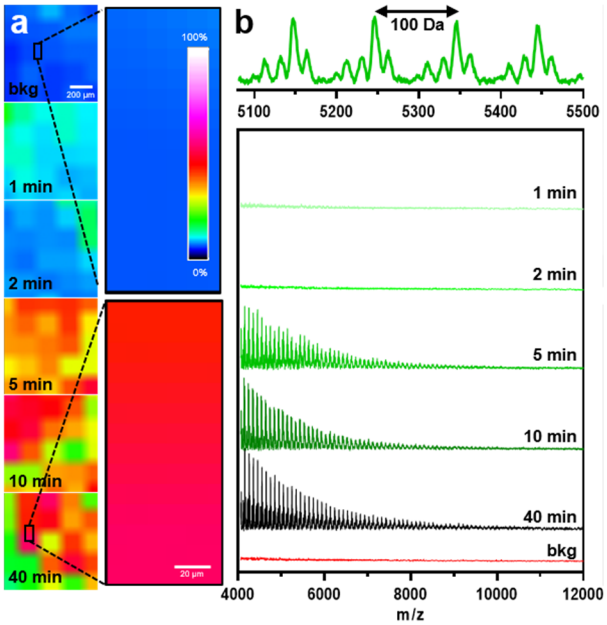

Figure 16. MALDI-IMS data for polymer brush hypersurface photolithography studies. **a.** MALDI-IMS map generated in the photochemical printer after 1-40 min irradiation with a mass filter of 5000 (± 500) *m/z*. Scale bars are 200 µm and 20 µm, respectively. **b.** Averaged MALDI spectra.

Exploring light-triggered polymerization as a method of 3D surface patterning
PIs: Gianneschi, Braunschweig, Mirkin

Over the course of the MURI, we have focused on developing synthetic tools to make bioactive peptide-polymer conjugates via harnessing light-triggered polymerization technique. Our hypothesis was that the light-triggered polymerization of bioactive peptide monomers could be exploited further for 3D printing of bioactive and patterned polymer materials, in which the peptide sequence and functionalities can be tuned for a desired property such as cell adhesion. To achieve this goal, first the synthesis and characterization of these peptide-polymer conjugates in bulk solution was explored and analyzed with a range of functional peptide vinyl monomers and polymer lengths, which can then be translated to varying heights of printed structures and functional inks. We successfully developed a new technique to generate well-defined peptide brush polymers *via* photoinitiated reversible addition-fragmentation transfer (photo-RAFT) polymerization (**Figure 17**).

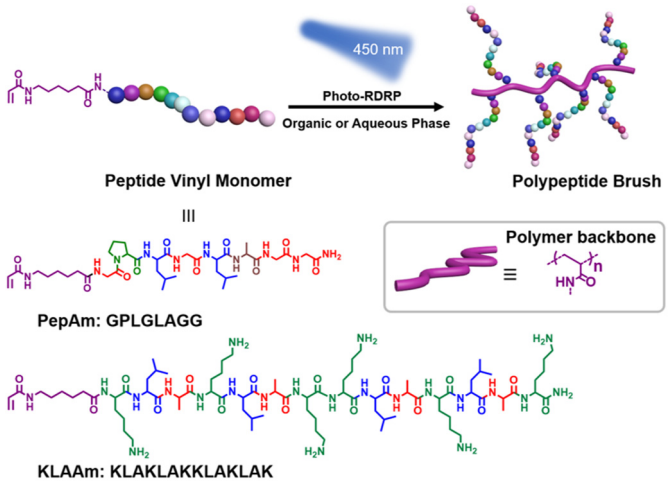

Figure 17. Synthesis of peptide brush polymers via photo-RAFT polymerization. A thermolysin-responsive amino acid sequence GPLGLAGG, and pro-apoptotic peptide KLAKLAKKLAKLAK.

To further achieve bioactive peptide-polymer conjugates with complex architectures, we developed a scalable and highly modular photoinitiated polymerization-induced self-assembly (photo-PISA) approach to functional peptides displayed as hydrophilic brushes on polymeric amphiphiles packed to form micellar nanoparticles. This is a robust approach to access block copolymer nanoparticles with a high-density display of functional peptides, tunable particle size, tunable peptide loading, and at scale (150 mg/mL). This method for packaging peptides was demonstrated with a proof-of-concept proapoptotic peptide (amino acid sequence: KLAKLAKKLAKLAK). These results clearly demonstrate the promise of exploiting nanoparticles with high peptide grafting densities to achieve enhanced proteolytic stability, cellular internalization, and cytotoxicity in comparison with free apoptotic peptides. We envision that many other functional peptides such as anti-fouling and adhesive peptides would be compatible with the photo-PISA approach to polymer brush amphiphile self-assemblies.

Surface-initiated Atom-transfer Radical Polymerization
PI: Braunschweig

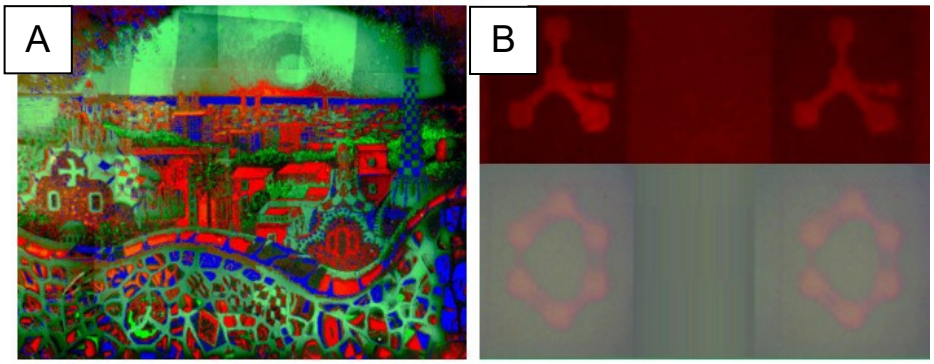

Figure 15. Application of Hypersurface Photolithography. (A) Composite of 75 microscopy images (25 images per channel) showing all three different fluorophores utilized to print an image of the Barcelona skyline. (B) Revealing the 2 hidden images under UV-light (top) and by applying heat (bottom) on the same area.

We investigated surface-initiated living photopolymerizations to create stimuli-responsive 6D block copolymer hypersurfaces. To this end, the kinetics of the surface-initiated atom-transfer radical photopolymerization (SI-ATRP) were investigated with our Hypersurface Photolithography platform, and we validated the ability to print the patterns of block copolymers consisting of ethylene glycol dimethacrylate (EGDMA) and *tert*-butyl methacrylate (*t*BMA), where the height of each block component was controlled independently at each pixel. To show the power of this technique, we printed a multicolor pattern depicting the skyline of Barcelona, reproduced at the microscale (**Figure 18C**). Building on this advance, we demonstrated a new method to embed orthogonal concealed images within 6D hypersurfaces using stimuli-responsive polymer brushes (**Figure 18D**) embedded within a forest of nonresponsive brushes. Under ambient conditions no pattern is seen, whereas upon exposure to UV light a tetrahedral carbon is observed. Alternatively, upon heating the brushes, a different pattern of a benzene ring emerges. Thus, a 6D hypersurface has been prepared, where pixels in the pattern are defined by *x, y* position, *h*, chemical composition, response to heat, and response to light. Moreover, we demonstrate a new paradigm in steganography, where multiple hidden images are embedded within the same hypersurface. Ultimately, however, by combining surface photochemistries and the new printer designs, this printing technique can now be extended to make polymer brush patterns for a wide array of applications in material science, biology, physics, and many other fields.

Light-directed Patterning of Functional Groups on Carbon Substrates
PIs: Wang, Mirkin, Brown

An important objective for this MURI project is the development of hierarchical ink chemistries for printing functional architectures. Toward this goal, **Wang** has developed a light-driven chemistry for covalently coupling functional groups to CNT thin-film substrates. The chemistry is driven by exciting the substrate with light, therefore offering unique opportunities to leverage the near-field light delivery capabilities of our 4D nanoprinter to potentially create high resolution molecular patterns and a diverse array of functional moieties since the chemistry is driven by

exciting the substrate rather than the molecules. Specifically, we show it is possible to use 565 nm light to drive the coupling reaction of aryl functional groups to single-walled carbon nanotubes. Our approach involves the synthesis and isolation of a chemically inert diazoether isomer that can be switched to its reactive form *in situ* by light that resonates with the optical frequency of the nanotube substrate (**Figure 19A**).[20] The results from spectroscopic monitoring of the reaction show that the *E*-isomer is completely chemical inert. However, excitation of the nanotube with light readily introduces covalently bonded *p*-nitroaryl functional groups to the carbon substrate. The successful covalent coupling is confirmed by the rise of a new photoluminescence peak at 1141 nm (**Figure 19B**), which is redshifted from that of the native exciton emission at 980 nm and characteristic of the electronic structure of the emitting center.

In a proof-of-concept experiment, **Wang** further demonstrated the patterning of the functional molecular groups using this light-driven chemistry.[21] We used the mapping capabilities of the confocal Raman microscope to pattern *p*-nitroaryl functional group arrays in an "M" shape on the SWCNT thin film. **Figure 19C** shows the Raman map of an "M" pattern due to the effective grafting of the functional groups. With this light-driven chemistry, it becomes possible to pattern molecular color centers, substantially increasing our capability of integrating optical and chemical functionalities for application in biosensing and quantum light sources, exciting new directions that the **Wang** group is exploring.

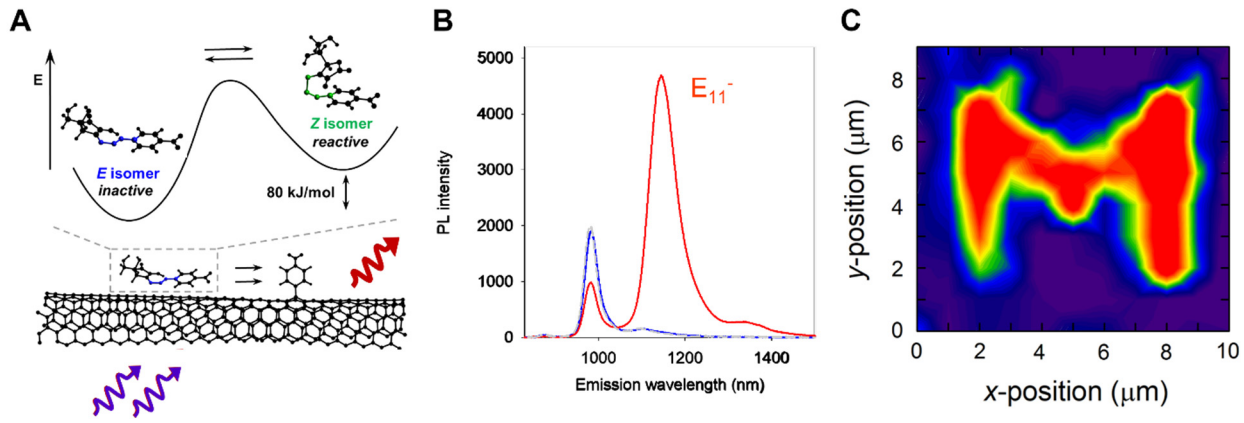

Figure 19. Carbon ink chemistry. (A) Schematic showing that light triggers covalent bonding of *p*-nitroaryl groups to a carbon substrate. (B) Excitation of the nanotube with 565 nm light turns on the reaction creating a bright photoluminescence peak (E_{11}^-) at 1141 nm (red). (C) Patterning of *p*-nitroaryl moieties on a carbon nanotube film with the designed "M" letter spectrally resolved by Raman mapping. These results are published in *J. Am. Chem. Soc.* and *Advanced Materials*.[20, 21]

PART II: Summary of accomplishments during the NCE period (12/15/2020 – 12/14/2021)

TA 1: Synergistic Efforts for Architecture

Cantilever-free Scanning Probe Microscopy

PIs: Brown

There were two major areas of progress in the no cost extension (NCE) period. The first was born out of the process of publishing the cantilever-free scanning probe microscopy paper which came out in early 2021.[22] During the review process, the reviewers raised interesting questions about whether the probe array would be suitable for performing mechanical characterization of the underlying substrate. The concept of using atomic force microscope probes for nanomechanics is quite well established, but it was unclear how a cantilever-free probe could be used in this regard. Thus, we performed a series of experiments and simulations to study how the deformation of cantilever-free probes would change depending on the relative stiffness of the probe, compliant backing layer, and substrate under study. Interestingly, we found that there were three regimes that were all distinct depending on these relative stiffnesses. In particular, if the probe and backing layer are substantially stiffer than the substrate, the probe is not able to image or characterize the substrate. If, instead, the probe is much stiffer than the substrate, but the substrate is commensurate in stiffness with the backing layer, then the probe array can be used for nanomechanical characterization and topographical imaging of the substrate. This is an exciting regime that includes samples composed of most glassy polymers and thus provides an interesting avenue to study composite nanomechanics. If, finally, the substrate is stiffer than the backing layer, only topographical imaging is possible. Understanding the delineation between these regimes was a powerful advance in considering how cantilever-free probes can be used to both pattern and functionally interrogate materials.

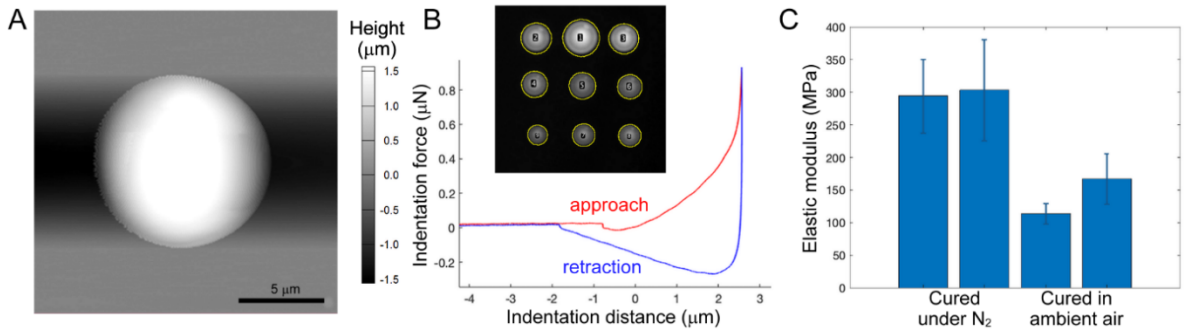

Figure 20: Scanning probe for iterative preparation and evaluation of nanoscale materials. (A) Topographical image of a polymer resin feature written by scanning probe lithography. (B) Force-displacement characterization of an individual resin feature. The shape of the approach/retraction curve can be analyzed to provide the mechanical properties of the polymer. Notably, this polymer feature was prepared using scanning probe lithography and is interrogated by scanning probe microscopy. The inset of this image shows a set of nine features written by scanning probe lithography that have been analyzed using an automated pipeline to identify their size. The center-to-center distance of these features is 25 µm. (C) Results of initial study using scanning probe characterization of nanoscale resins. Resin photocured in nitrogen has over twice the average elastic modulus as resin cured in ambient conditions.

On the topic of using a single probe to pattern and interrogate materials, in a second area of progress, we also explored iteratively writing and characterizing patterned features. In particular, the ability to pattern materials and then characterize them with the same probe array could be enabling from the perspective of high throughput screening. In order to test this idea using a model system, we developed an approach to use scanning probes to pattern polymers, photocure them, and then characterize their mechanical properties. Using this process, we found that it was possible to perform materials synthesis and characterization using the same system in a closed-loop fashion. These advances provide a powerful incentive to close the loop using cantilever-free scanning probes to obtain massive throughput in material screening (**Figure 20**).

Controlling Intracellular Machinery via PPL-Based Molecular Patterning

PIs: Mirkin, Mrksich

Cells respond to their surroundings by transducing mechanical force into biochemical cues that activate pathways crucial for a wide spectrum of cellular functions. During this reporting period, we continued to examine how cell membrane tensions generated within the cytoskeleton affect endocytosis. Briefly, PPL arrays were inked with mercaptohexanoic acid (MHA) and loaded into a PPL instrument for surface printing (**Figure 21**). Using PPL, we deposited MHA onto gold-coated glass slides, and we then backfilled the bare gold with a bio-inert thiolated polyethylene glycol (PEG) molecule that prevents the non-specific adsorption of proteins onto the unpatterned regions. Then, fibronectin was attached to the MHA patterns, and fibroblast cells were cultured

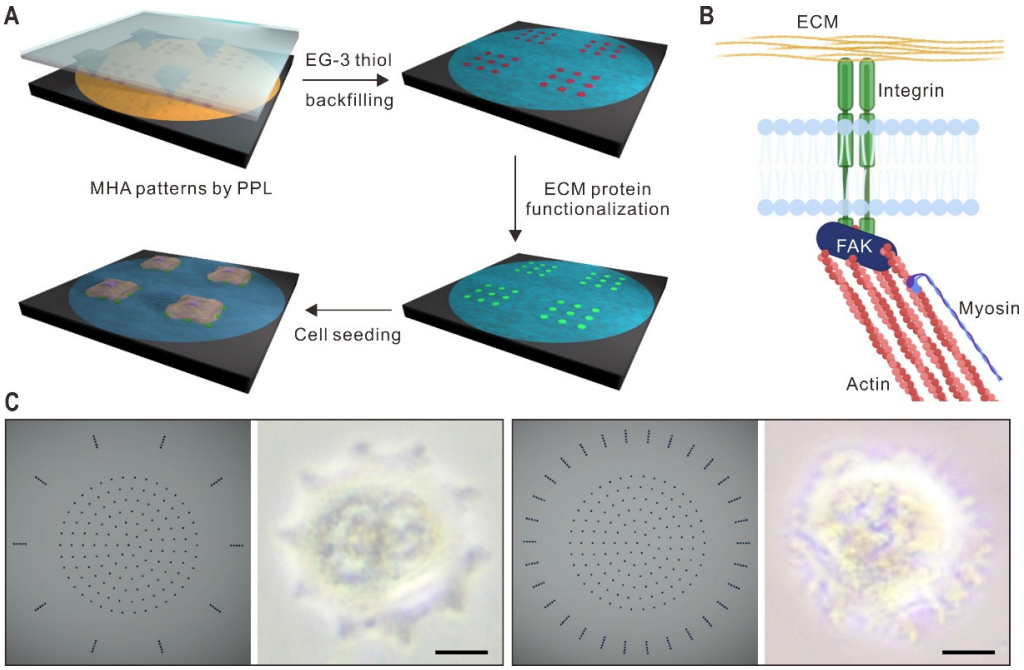

Figure 21. (A) A schematic showing the key steps for generating the cellular substrates utilized in this study: deposition of MHA, backfilling with PEG, protein immobilization on the pattern regions, and cell attachment to the patterns. (B) Illustration of mechanical tensions exerted on the ECM by cells through focal adhesion contacts established by the myosin-actin interaction. (C) Pattern designs (left) and optical micrographs (right) of cell adhesion and cell morphological changes corresponding to the underlying pattern designs. Scale bars: 10 μm.

and immobilized on these substrates. After a 24-h incubation step, the cells were spread over the fibronectin patterns; their shapes were dictated by the shapes of the underlying patterns (5, 20, or 35-point circles). Previously, we established that (compared to the cells on the 35-point patterns) the cells on the 5-point circular patterns: 1) were more contractile; 2) exhibited elevated levels of kinase phosphorylation at tyrosine 397 (FAK[pY397], an established response to increased actin contractility); and 3) had a higher Young's modulus (*i.e.*, were more stiff).

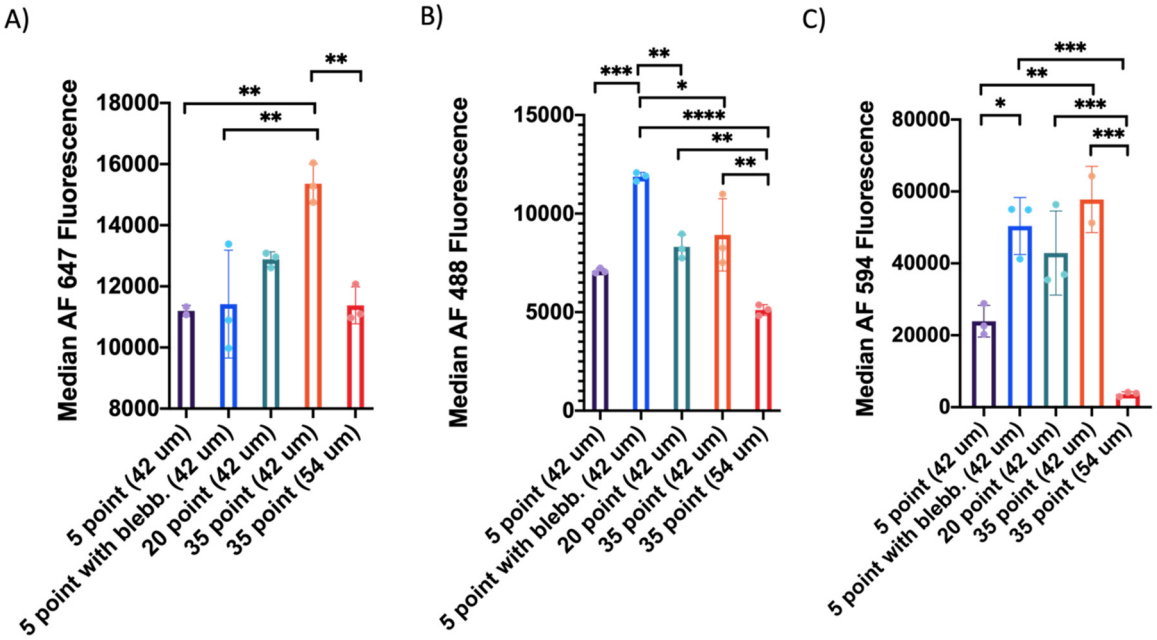

Figure 22. Flow cytometric analysis showing the median fluorescent intensity as an indication of the relative amount of cholera toxin uptake (labeled, AF 647) and the presence of labeled antibodies against caveolae (AF 488) and clathrin (AF 594).

This year, we performed experiments looking at how a fluorophore-labeled cholera toxin (CTX) protein was taken up by these cells, which were experiencing different cellular tensions/forces, using flow cytometry. The data reveal that the cells seeded on the 5-point circles (highest contractility) took up the least CTX, while those seeded on the 35-point circles (lowest contractility) took up the most CTX (**Figure 22A**). Next, we stained the cells with labeled antibodies against clathrin and caveolin and found that fewer of these markers were present with the cells that exhibited increased contractility (**Figure 22B, C**). Moreover, when the cells were seeded on 35-point circular patterns with a larger spreading area (54 μm vs. 42 μm), and thus increased spacing between their external features, they took up less CTX and less clathrin and caveolin was observed. And, when we treated the cells on the 5-point circular patterns with blebbistatin, a myosin inhibitor, CTX uptake as well as clathrin and caveolin levels increased. These results point to the fact that elevated contractility decreases uptake and endocytosis activity and suggests that these processes can be altered through direct manipulation of the geometry of the underlying protein pattern via nanotechnology. This method can be used to study complex biological systems and applied in a variety of applications in cellular engineering.

TA2: Synergistic Efforts for Ink Chemistry

Thermoresponsive Materials Patterning – Development of Hypersurfaces
PIs: Braunschweig, Gianneschi

During the NCE period, the **Braunschwig** group utilized novel printing tools to further explore stimuli responsive hypersurfaces and glycan microarrays. With respect to the stimuli-responsive surfaces, we reported new approaches to concealing information that rely upon creating microscale patterns composed of different polymer brushes, where at least one has an optically detectable response to external stimuli (**Figure 23**).

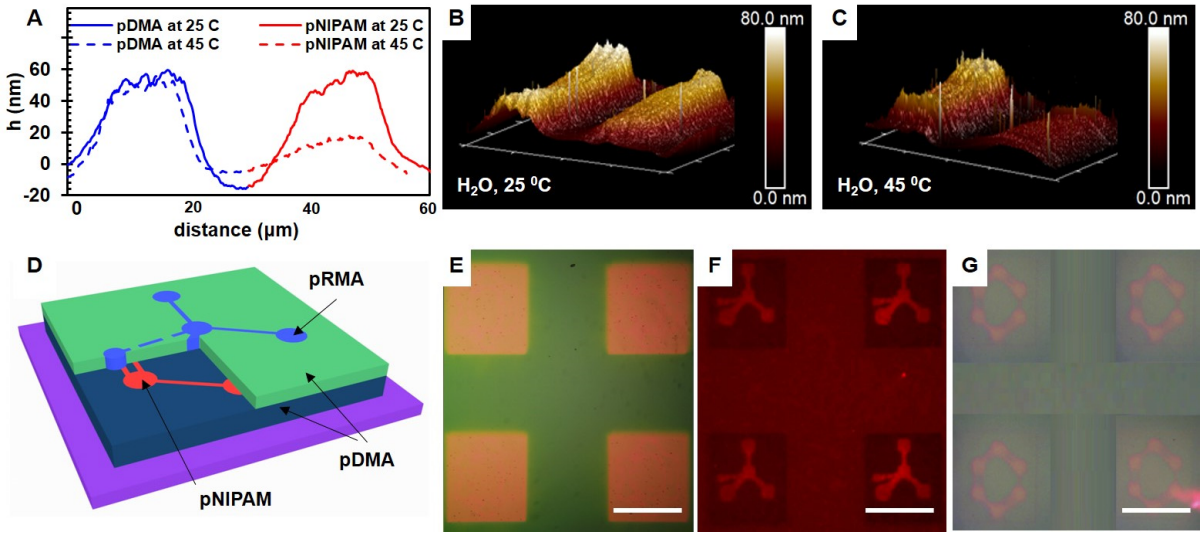

Figure 23. Evolution of massively-parallel scanning probe lithography (SPL). (A) Graph shows the changes in height of features of different polymer brushes (red is pNIPAM and blue is pDMA) at 25 and 45 °C. (B) 3D image of substrate composed of pDMA (left) and pNIPAM taken in H_20 by liquid AFM at 25 °C. (C) 3D image of substrate composed of pDMA (left) and pNIPAM taken in H_20 by liquid AFM at 45 °C. (D) Structure of the 6D hidden image. (E) Optical image of the 6D hidden image. (F) Revealing the 1st hidden image under UV-light. Fluorescence image of the hidden image (λ_{ex} =530–550 nm, barrier filter λ_{em} =575nm). (G) Revealing 2nd hidden image by applying heat in H_2O. Scale bar is 200 μm.

In the first, thermoresponsive poly(*N*-isopropylacrylamide) (pNIPAM) brushes are patterned alongside nonresponsive poly(*N*,*N*-dimethylacrylamide) (pDMA) polymers of the same height. Upon heating in water above their lower critical solution temperature (LCST) of 32 °C, the pNIPAM brushes collapse, while the pDMA brushes remain unchanged, thereby resulting in a change in contrast visible to the naked eye that reveals the hidden message. While such a steganographic system is conceptually simple, achieving it is not and requires addressing several major challenges in brush polymer and surface chemistries. Essentially, this application demands a printing method that can control six independent parameters of each pixel in the polymer brush pattern—the *x* and *y* position on the surface, the height of the brushes, their chemical composition, and their response to heat and light. By our recently coined terminology, such a pattern would be designated a "6D hypersurface."

Surface-Initiated Controlled Radical Polymerization
PIs: Braunschweig, Gianneschi

Another application of the hypersurface printing technology involved developing new surface-initiated polymer chemistry to create multiplexed glycan microarrays that reproduce the dense glycan presentation found in the glycocalyx. To accomplish this, we combined Hypersurface Photolithography (HP) (**Figure 24A**), with a reaction that we term "grafted-to/grafted-from radical photopolymerization" (GTGFRP, **Figure 24B**), in which the glycans are grafted to a polymer chain as it grows grafted from a surface and use the resulting glycan microarrays to explore systematically the role of grafting density and polymer height on K_d. The result of these efforts is a powerful new approach for creating glycan microarrays, a fuller understanding of how glycopolymer architecture can be modulated to control K_d, and multiplexed glycopolymer microarrays with sub-1 fm K_ds to ConA—the strongest binding between GBPs and glycan arrays yet reported. To explore the brush growth rates, a set of surfaces were patterned, where, in each surface, a single parameter is varied and all others are held constant. First, the [EGDMA] was varied from 520 to 1560 mm, while [TPO], *hv*, and [PETT] were held constant (**Figure 24E**). We next investigated how the introduction of the alkene-functionalized glycan, pent-4-enyl-α-d-mannopyranoside (Man-5) into the reactive solution affected polymer growth rate and confirmed that the glycan is incorporated into the growing brushes. To do so, we printed the same 16-feature patterns onto the thiol-terminated substrates, and [Man-5] was varied from 0–500 μm (**Figure 24E**). Glycan incorporation into these polymer brushes was confirmed by XPS and micro-FTIR analysis. A series of assays were carried out to examine the relationships between polymer architecture and their binding to FITC-ConA (**Figure 24G**). Using the fluorescence data, we determined the K_ds between ConA and the glycopolymer brushes for all 72 combinations of brushes and ConA solutions. We observed decreasing K_d with increasing glycan density and increasing *h*. In our previous report, the lowest [ConA] observed to bind to Man-5 monolayers was at a [ConA] of 48 nm with a K_d of 28 nm, while here, the lowest [ConA] observed to bind to Man-5 glycopolymers was at a solution concentration of 10^{-4} pm with a K_d of 0.3 fm, resulting in binding that is 10^{-7} m stronger than the monolayers of Man-5. These K_ds are $\approx 10^{-7}$ m lower than galactosides grafted to linear polymers by aminooxy conjugation, and 10^{-8} m lower than the binding of *ricinus communis agglutinin I* to galactosides bound to linear polymers via thiol–ene photochemistry. The fluorescence values were also used quantitatively to analyze the binding cooperativity of ConA with the surface glycopolymer. The Hill coefficient was determined to be −0.37, whose value of <1 indicates negative cooperativity in binding that is in good agreement with prior reports that ConA binds with negative cooperativity to polyvalent ligands.

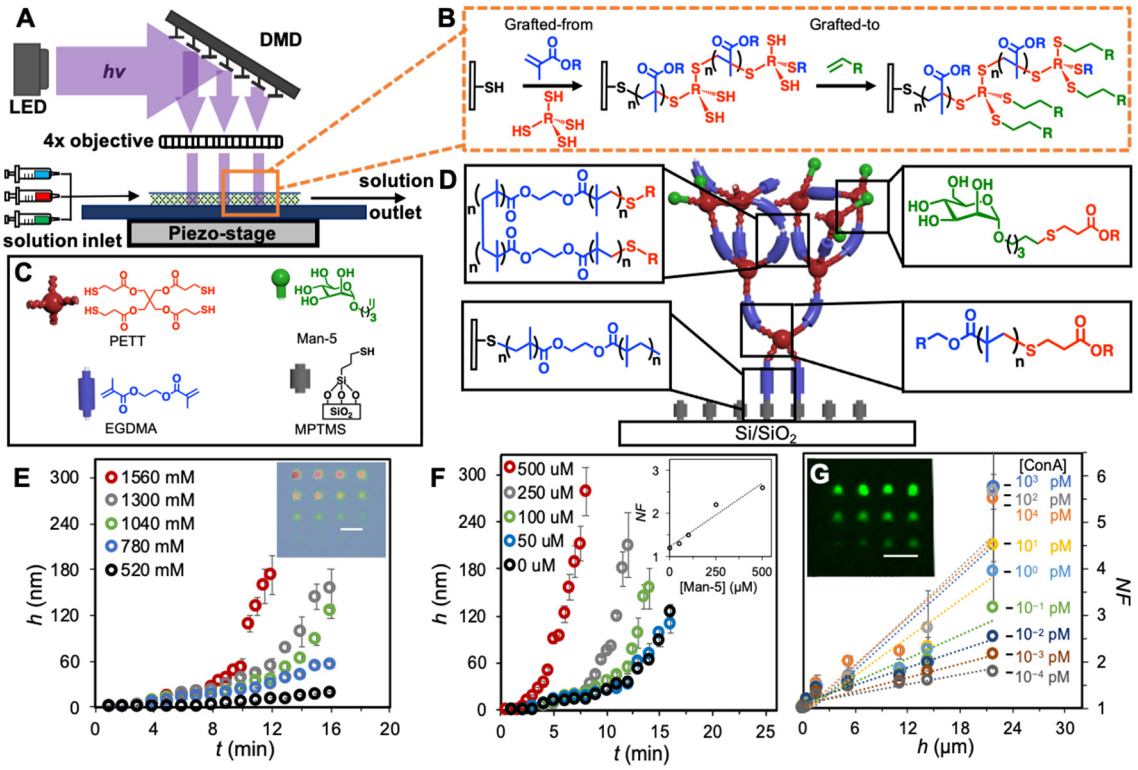

Figure 24. (A) Hypersurface photolithography was used to patterned copolymer brushes from surfaces. (B) Grafted-to/grafted-from radical photopolymerization (GTGFRP) from a thiol-terminated surface. (C) Constituents of the glycopolymer brush represented in (D) prepared by the GTGFRP reaction. (D) Model of the glycopolymer brush formed by the GTGFRP and the chemical bonds that occur. (E) Growth rates of the glycopolymer brushes were studied by systematically varying monomer concentration ([EGDMA]) and light exposure time, *t*. An optical image of a 4 × 4 pattern is shown in the inset with a scale bar of 100 μm. (F) Relationship between height, *h*, and irradiation time for glycopolymers composed of EGDMA, PETT. The concentration of α-Man was varied systematically to understand how it affected growth rate. The inset shows the effect varying [Man-5] on normalized fluorescence (NF) with polymer brushes with heights of 110 ± 10 nm. (G) Binding study performed by varying ConA concentration on surfaces with glycopolymer brushes with varying *h*. The inset is fluorescence microscopy of ConA bound to Man-5 glycopolymers with a scale bar of 100 μm.

Controlling Local Chemistry of Soft Materials for Cell Migration

PIs: Mirkin

In vivo both chemical and mechanical factors in the extracellular matrix play a role in regulating cellular behavior. In order to investigate the effect of both of these variables, new patterning strategies for multiplexed soft materials are required. Typically patterning multiplexed soft materials relies on sequential patterning steps, which involve time-intensive washing and re-alignment steps. Here we propose to use wavelength specific photochemistries for the functionalization of biochemical ligands and the modulation of mechanical properties within a single substrate, enabling a combinatorial study where libraries of chemical and mechanical gradients can be patterned, and cellular responses can be measured. Cantilever-free scanning probe

lithography (*i.e.*, BPL) is capable of incorporating different wavelengths in one system, which allows for the continuous printing of heterogeneous materials.

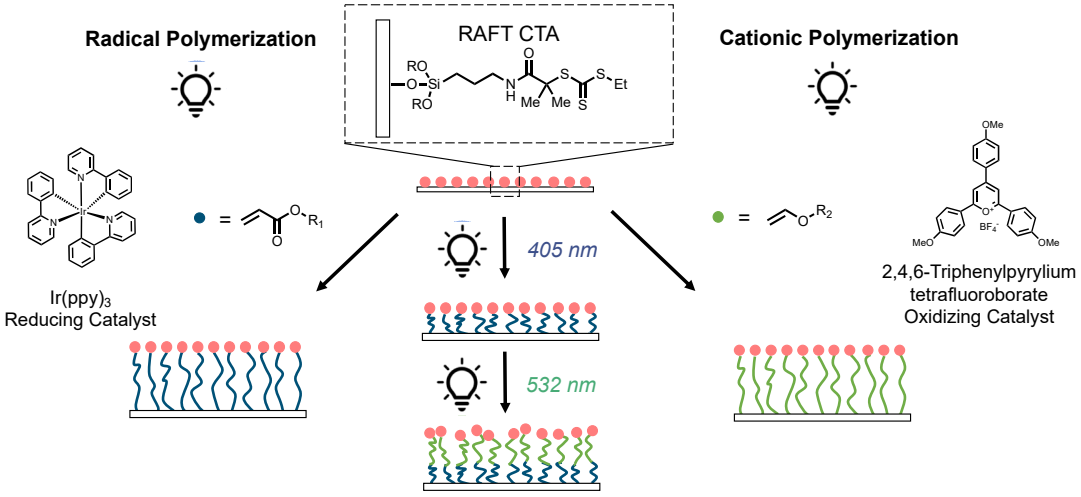

Figure 25. Scheme showing the polymerization mechanism for Reversible Addition-Fragmentation chain Transfer (RAFT) using a chain-transfer agent (CTA) specified by wavelength of irradiation can lead to controlled features of different heights and compositions.

To enable this, we sought to use wavelength selective controlled polymerization developed by Fors and coworkers where a chain transfer agent could initiate radical or cationic polymerization depending on the wavelength of light exposed to the surface.[23] Specifically, in the presence of an oxidizing catalyst, they showed that blue light can initiate the controlled radical polymerization of acrylate monomers and in the presence of a reducing catalyst, green light can initiate cationic polymerization of vinyl ether monomers (**Figure 25**).

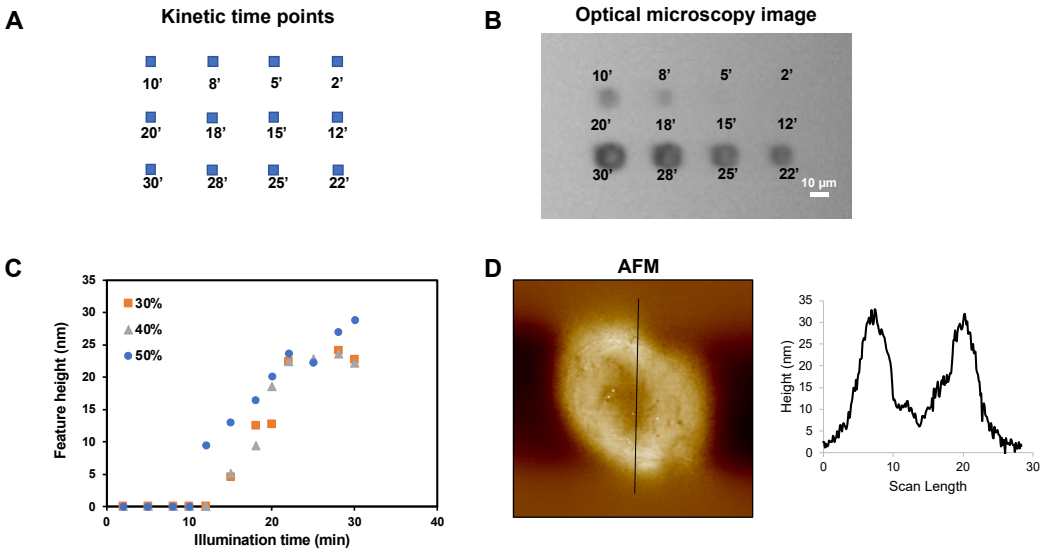

Figure 26. A) Array of time points used to study polymerization kinetics of NIPAM under blue light irradiation. B) Optical micrograph of patterned features shows increased optical contrast at longer time points. After 12 minutes, features begin to get overexposed. C) Height profiles at varying intensities were measured using AFM, indicating intensity had a marginal impact on feature height. D) AFM characterization indicated a feature size of 30 nm at 30-minute time points.

To enable surface patterning, silicon wafers were functionalized with silanated 2-(Dodecylthiocarbonothioylthio)-2-methylpropionic acid (DDMAT), a chain transfer agent (CTA) that can initiate cationic and radical polymerizations. This functionalization enables the grafting-from polymerization of polymer brushes with composition controlled by the irradiation wavelength. Preliminary studies reported herein focused on the controlled polymerization of blue-light initiated systems. First, a solution consisting of n-isopropyl acrylamide (NIPAM) monomer and Irridium catalysts (*i.e.,* $Ir(ppy)_3$) was drop casted onto the DDMAT-functionalized surface. Using a digital micromirror device, the surface was irradiated with 405 nm light at varying intensities and exposure times, yielding polymer brushes of various height (**Figure 26**). These patterned surfaces enabled the facile study of how irradiation conditions affected the kinetics of surface polymerization.

Development of a New Bioink Chemistry Using CRABP2

PIs: Mrksich

The **Mrksich** group developed a new bioink chemistry based on the covalent linkage of Cellular Retinoic Acid Binding Protein 2 (CRABP2) and a synthetic retinoid bearing an arylfluorosulfate group, which uses sulfur fluoride exchange click chemistry to covalently inhibit CRABP2. This reaction is fast (approximately 3,600 $M^{-1}s^{-1}$) and stable. The development of a third chemistry will greatly increase the range of bioink architectures we can prepare. This work was recently published, incorporating additional work conducted in this reporting period.[19]

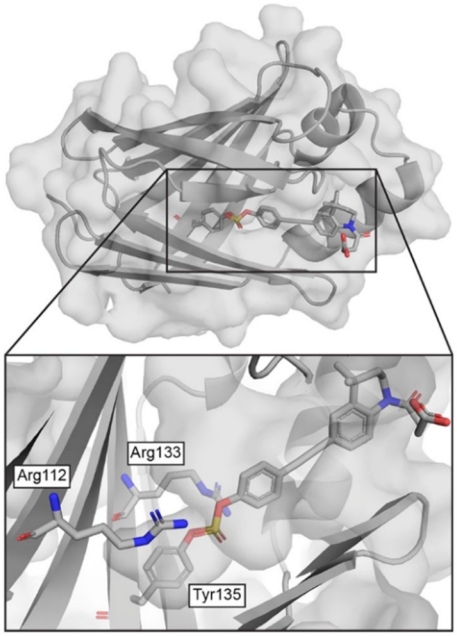

Figure 27. Crystal structure at 2.0 Å of the CrabTag-inhibitor complex. Tyr135 forms a covalent bond with the arylfluorosulfate electrophile within the synthetic retinoid inhibitor, where the resulting Tyr ~ Arg ~ Arg motif is specified.

As noted in the previous reporting period, we developed a new bioink chemistry based on the covalent linkage of Cellular Retinoic Acid Binding Protein 2 (CRABP2) with a synthetic retinoid bearing an arylfluorosulfate group, which uses sulfur fluoride exchange click chemistry to covalently inhibit CRABP2. In this NCE period, we elaborated on the work, characterizing its kinetics, structure, and applications, and published the work. After synthesizing the small molecule inhibitor, we obtained a crystal structure of the inhibitor bound to CRABP2, verifying that it attaches at the expected atom in the active site of the enzyme (**Figure 27**.)

Next, we characterized the kinetics of the reaction between a fluorescently tagged version of the inhibitor and CRABP2 (**Figure 28**). The results show that the reaction produces the expected mass, and that it rapid, with a K_{eff} = 3,600 $M^{-1}s^{-1}$.

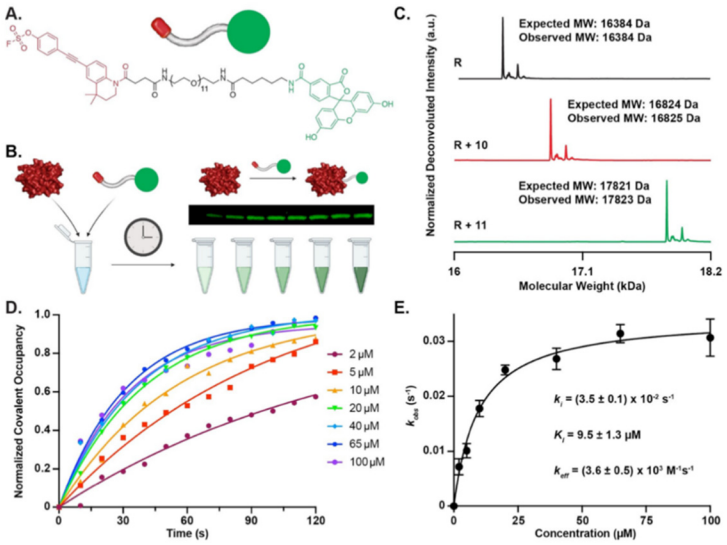

Figure 28. Kinetic characterization for the reaction of (A) the fluorescently labeled synthetic retinoid inhibitor. (B) Reaction of CrabTag with the inhibitor was stopped at different time points using Laemmli buffer. Reaction products were separated using SDS-PAGE and the fluorescent product band was quantitated using ImageJ. (C) Deconvoluted protein mass spectrometry data quantifying the molecular weight of CrabTag (R, black) before and after complexation with either the unlabeled inhibitor (red) or labeled inhibitor (green). (D) Fraction of covalently occupied CrabTag protein plotted for each linker concentration at discrete time points to give kobs. (E) The k_{obs} data were plotted relative to the linker concentrations in a Michaelis-Menten analysis and gave constants k_i, K_I, k_{eff}. All plots and values have error represented as SEM.

We showed that this chemistry could be used with two other ink chemistries in a one-pot reaction to generate precisely defined, elaborate structures composed of both proteins and small molecules, in a short period of time (less than two hours) (**Figure 29**). Using a fluorescently labeled small molecule and gel electrophoresis to monitor the progress of the reactions, we could observe the evolution of the reactions and map out the order of connectivity and kinetics of each step.

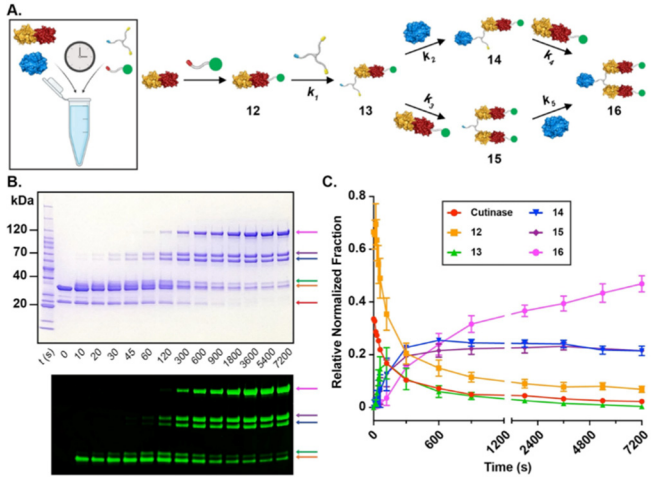

Figure 29. Monitoring one-pot megamolecule assembly. (A) Scheme of the one-pot multi-protein assembly synthesis from building blocks into product 16. (B) Top: Brightfield SDS-PAGE of the reaction over a two-hour time scale. Benchmark protein ladder for relative scale. Bottom: Fluorescent image of SDS-PAGE (Red arrow, Cutinase; Orange arrow, 12; Green arrow, 13; Blue arrow, 14; Purple arrow, 15; Magenta arrow, 16). (C) Plot showing the relative abundance of all reaction intermediates over time as quantified using both brightfield and fluorescent SDS-PAGE.

This work adds to the tools available for the rapid generation of complex, multifunctional bioinks. In this NCE period, we published the work described here, where we synthesized and characterized four-armed megamolecules, further expanding our ability and understanding of methods for generating complex megamolecule bioinks.[16]

Exploring Light-triggered polymerization as a method of 3D surface patterning
PIs: Gianneschi, Braunschweig, Mirkin

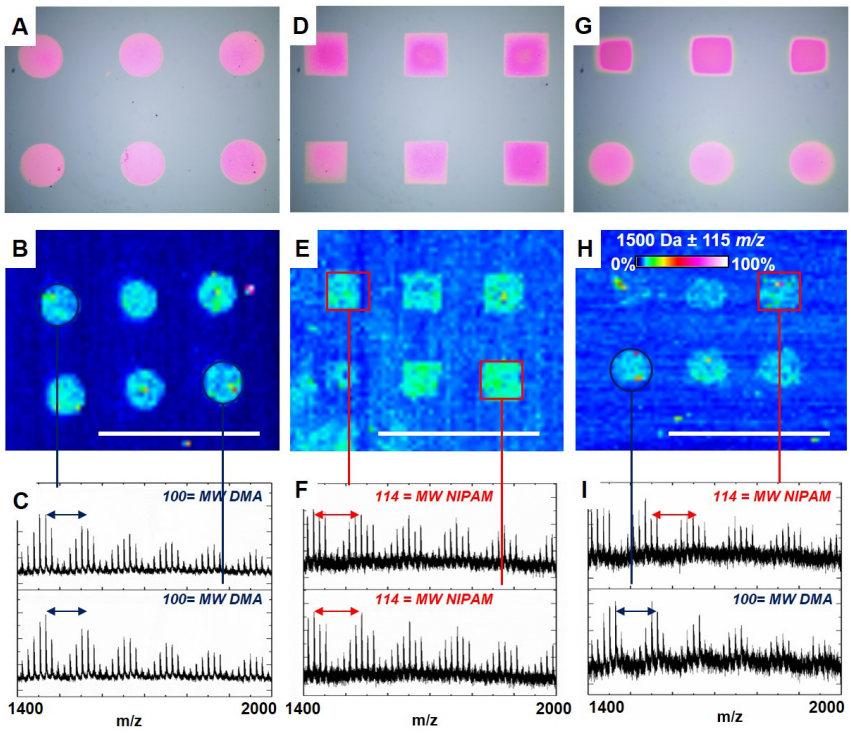

Figure 30. MALDI-IMS data for polymer brush surfaces. **A.** Optical image, **B.** MALDI-IMS colormap, and **C.** average mass spectra of PDMA brushes. **D.** Optical image, **E.** MALDI-IMS colormap, and **F.** average mass spectra of PNIPAM brushes. **G.** Optical image, **H.** MALDI-IMS colormap, and **I.** average mass spectra of PNIPAM and PDMA multiplex brushes. All MALDI-IMS mass filtered maps are shown with a mass filter of 1500 (± 115) *m/z*. Scale bar is 1000 µm.

During the NCE period, we built upon our previous work on photopatterned poly(methyl methacrylate) (PMMA) surfaces, and shifted focus to patterning poly(dimethylacrylamide) and poly(N-isopropyl acrylamide). In addition to characterization performed by the **Braunschweig** group, we have utilized MALDI-IMS to analyze these polymer surfaces patterned with PDMA, PNIPAM, and a multiplex pattern of the two polymers (**Figure 30**).

Using a mass filter of 1500 Da ± 115 *m/z*, the colormap of each surface polymer shows the photopatterned regions containing PNIPAM, PDMA, and a multiplex of the two polymers with high spatial resolution (**Figure 30A-I**). Both PNIPAM and PDMA show complex fragmentation patterns, but the peak spacing corresponds to the monomer mass in each case, confirming that the desired polymers were indeed synthesized (**Figure 30C, F, I**). Ultimately, this research enabled a new method to encrypt data within 5D and 6D hypersurfaces using stimuli-responsive polymer brushes embedded within a forest of nonresponsive brushes.

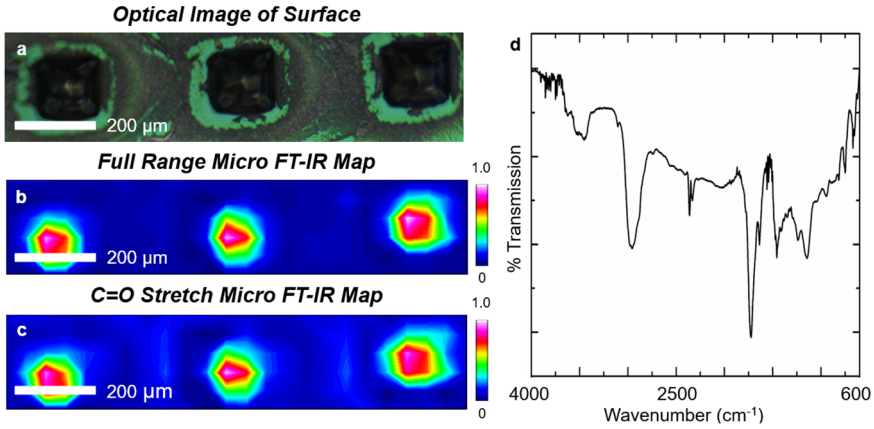

Figure 31. Micro-FTIR data for polymer patterned surface composed of EGDMA, PETT, and Man-5 **a.** Optical image. **b.** Full range (4000-600 cm^{-1}) map. **c.** Filtered map (1800-1650 cm^{-1}). **d.** Average FT-IR spectrum of one patterned square.

Additionally, the **Gianneschi** and **Braunschweig** groups utilized micro-Fourier transform infrared resonance (FTIR) spectroscopy to study glycopolymer microarrays (**Figure 31**). The arrays were prepared via a new surface-initiated polymerization, termed "grafted-to/grafted-from radical photopolymerization" that was optimized using hypersurface photolithography, a printing strategy that substantially accelerates reaction discovery and optimization. The rapid development of this new chemistry and the systematic investigation of brush height and grafting density are all enabled by a new chemical printer that accelerates the discovery and optimization timeline, which is demonstrated herein by the >400 different reaction conditions for growing the polymer brushes whose growth and binding were analyzed. Quantitative binding studies explain the cause of the unprecedented avidity to these polymer brushes. The new chemistry and the understanding of the underlying binding process that we report could usher in a new era in glycobiology, where glycan-binding proteins can now be detected at medically- and biologically relevant concentrations.

Peptide-brush polymers (PBPs), wherein every side chain of the polymers is peptidic, represent a new class of proteomimetic with unusually high proteolytic resistance while maintaining bioactivity (**Figure 32**). Here, we sought to determine the origin of this behavior and to assess its generality via a combined theory and experimental approach. A series of PBPs with various polymer backbone structures were prepared via photo-RAFT and examined for their proteolytic stability and bioactivity. We discovered that an increase in the hydrophobicity of the polymer backbones is predictive of an elevation in proteolytic stability of the side-chain peptides. Computer simulations, together with small-angle X-ray scattering (SAXS) analysis, revealed globular morphologies for these polymers, in which pendant peptides condense around hydrophobic synthetic polymer backbones driven by the hydrophobic effect. As the hydrophobicity of the polymer backbones increases, the extent of solvent exposure of peptide cleavage sites decreases, reducing their accessibility to proteolytic enzymes. This study provides insight into the important

factors driving PBP aqueous-phase structures to behave as globular, synthetic polymer-based proteomimetics.

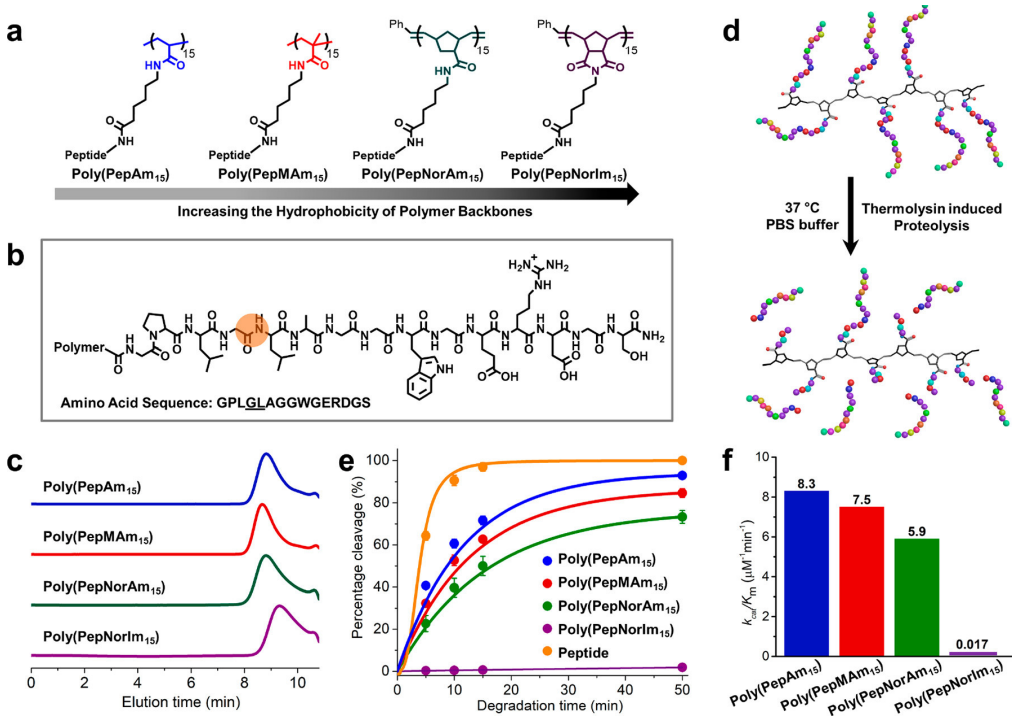

Figure 32. Polymer backbone structures of PBPs determine the proteolytic stability of the peptide side chains. **a.** Structures of the set of PBPs. **b.** Structure of GPLGLAGGWGERDGS peptide used in this study. **c.** Gel permeation chromatography traces of PBPs. **d.** Schematic illustration of proteolytic digestion of peptide-brush polymers in the presence of thermolysin. **e.** Proteolysis kinetics of PBPs and the free peptide revealed by HPLC. **f.** Catalytic efficiency (kcat/Km) of thermolysin in proteolysis of PBPs.

CONCLUDING REMARKS

The research efforts and results presented here are the culmination of a multi-year investment to realize the ability to create 3D and 4D Materials using cantilever-free lithographic technologies. These methods allow for the efficient and cost-effective patterning of nanostructures over square centimeter areas by the direct deposition of materials. The work proposed in the original MURI proposal was ambitious. As evidenced by our annual reports, we have made significant progress towards our original goals. Regarding the development of patternable inks, we have synthesized and studied novel megamolecules, antibody-enzyme conjugates, and peptide-based polymers. Towards advancing printer architecture, we have created uniform apertures for beam-pen lithography (BPL) and achieved few pen actuation using CNT-based elastomers for polymer pen lithography (PPL). In addition, new technologies have arisen from this grant including the development of cantilever-free atomic force microscopy, electrochemical PPL, and high-area rapid printing (HARP), the highest-ever-throughput, macro-scale 3D printing technique.

REFERENCES

1. Huo, F. W.; Zheng, G. F.; Liao, X.; Giam, L. R.; Chai, J. A.; Chen, X. D.; Shim, W. Y.; Mirkin, C. A., Beam pen lithography. *Nat. Nanotechnol.* **2010,** *5* (9), 637-640.

2. Huo, F. W.; Zheng, Z. J.; Zheng, G. F.; Giam, L. R.; Zhang, H.; Mirkin, C. A., Polymer pen lithography. *Science* **2008,** *321* (5896), 1658-1660.

3. Walker, D. A.; Hedrick, J. L.; Mirkin, C. A., Rapid, large-volume, thermally controlled 3D printing using a mobile liquid interface. *Science* **2019,** *366* (6463), 360-364.

4. Xie, Z.; Gordlichuk, P.; Lin, Q. Y.; Meckes, B.; Chen, P. C.; Sun, L.; Du, J. S. S.; Zhu, J. H.; Liu, Y.; Dravid, V. P.; Mirkin, C. A., Solution-Phase Photochemical Nanopatterning Enabled by High-Refractive-Index Beam Pen Arrays. *ACS Nano* **2017,** *11* (8), 8231-8241.

5. Oh, E.; Golnabi, R.; Walker, D. A.; Mirkin, C. A., Electrochemical Polymer Pen Lithography. *Small* **2021,** *17* (28), 2100662.

6. Cabezas, M. D.; Meckes, B.; Mirkin, C. A.; Mrksich, M., Subcellular Control over Focal Adhesion Anisotropy, Independent of Cell Morphology, Dictates Stem Cell Fate. *ACS Nano* **2019,** *13* (10), 11144-11152.

7. Huang, Z. J.; Li, L.; Zhang, X. A.; Alsharif, N.; Wu, X. J.; Peng, Z. W.; Cheng, X. Y.; Wang, P.; Brown, K. A.; Wang, Y. H., Photoactuated Pens for Molecular Printing. *Adv. Mater.* **2018,** *30* (8).

8. Li, L.; Huang, Z. J.; Wang, Y. H.; Brown, K. A., Design of Elastomer-CNT Film Photoactuators for Nanolithography. *Polymers* **2019,** *11* (2), 314.

9. Horiuchi, N., Photoactuated printing. *Nature Photonics* **2018,** *12* (3), 123-123.

10. Modica, J. A.; Lin, Y.; Mrksich, M., Synthesis of Cyclic Megamolecules. *J. Am. Chem. Soc.* **2018,** *140* (20), 6391-6399.

11. Zhou, S. W.; Metcalf, K. J.; Bugga, P.; Grant, J.; Mrksich, M., Photoactivatable Reaction for Covalent Nanoscale Patterning of Multiple Proteins. *ACS Appl. Mater. Inter.* **2018,** *10* (47), 40452-40459.

12. Bugga, P.; Mrksich, M., Dynamic substrates for cell biology. *Curr. Opin. Colloid In.* **2018,** *38*, 80-87.

13. Li, S. H.; Mrksich, M., An Unusual Salt Effect in an Interfacial Nucleophilic Substitution Reaction. *Langmuir* **2018,** *34* (23), 6713-6718.

14. Taylor, E. L.; Metcalf, K. J.; Carlotti, B.; Lai, C. T.; Modica, J. A.; Schatz, G. C.; Mrksich, M.; Goodson, T., Long-Range Energy Transfer in Protein Megamolecules. *J. Am. Chem. Soc.* **2018,** *140* (46), 15731-15743.

15. Taylor, E. L.; Metcalf, K. J.; Carlotti, B.; Lai, C. T.; Modica, J. A.; Schatz, G. C.; Mrksich, M.; Goodson, T., 3rd, Long-Range Energy Transfer in Protein Megamolecules. *J. Am. Chem. Soc.* **2018,** *140* (46), 15731-15743.

16. Zhou, S. W.; He, P.; Dhindwal, S.; Grum-Tokars, V. L.; Li, Y.; Parker, K.; Modica, J. A.; Bleher, R.; Dos Reis, R.; Zuchniarz, J.; Dravid, V. P.; Voth, G. A.; Roux, B.; Mrksich, M., Synthesis, Characterization, and Simulation of Four-Armed Megamolecules. *Biomacromolecules* **2021,** *22* (6), 2363-2372.

17. Li, P.; Modica, J. A.; Howarth, A. J.; Vargas, E. L.; Moghadam, P. Z.; Snurr, R. Q.; Mrksich, M.; Hupp, J. T.; Farha, O. K., Toward Design Rules for Enzyme Immobilization in Hierarchical Mesoporous Metal-Organic Frameworks. *Chem* **2016,** *1* (1), 154-169.

18. Metcalf, K. J.; Kimmel, B. R.; Sykora, D. J.; Modica, J. A.; Parker, K. A.; Berens, E.; Dai, R.; Dravid, V. P.; Werb, Z.; Mrksich, M., Synthetic Tuning of Domain Stoichiometry in Nanobody-Enzyme Megamolecules. *Bioconjug. Chem.* **2021,** *32* (1), 143-152.

19. Kimmel, B. R.; Mrksich, M., Development of an Enzyme-Inhibitor Reaction Using Cellular Retinoic Acid Binding Protein II for One-Pot Megamolecule Assembly. *Chem-Eur J.* **2021,** *27* (71), 17843-17848.

20. Powell, L.; Wang, Y. H., Chirality-selective functionalization of semiconducting carbon nanotubes with a conformation switchable molecule. *J. Am. Chem. Soc.* **2017,** *139* (36), 12533-12540.

21. Huang, Z. J.; Powell, L. R.; Wu, X. J.; Kim, M.; Qu, H. R.; Wang, P.; Fortner, J. L.; Xu, B. B.; Ng, A. L.; Wang, Y. H., Photolithographic Patterning of Organic Color-Centers. *Adv. Mater.* **2020,** *32* (14), 1906517.

22. Cao, W.; Alsharif, N.; Huang, Z.; White, A. E.; Wang, Y.; Brown, K. A., Massively parallel cantilever-free atomic force microscopy. *Nature Communications* **2021,** *12* (1), 393.

23. Kottisch, V.; Michaudel, Q.; Fors, B. P., Photocontrolled Interconversion of Cationic and Radical Polymerizations. *J. Am. Chem. Soc.* **2017,** *139* (31), 10665-10668.